ACS Sustainable Chemistry & Engineering

Research Article

pubs.acs.org/journal/ascecg

# Nanotechnology in Solar and Biofuels

Hema Ramsurn and Ram B. Gupta*

Department of Chemical Engineering, Auburn University, Auburn, Alabama 36849-5127, United States

**ABSTRACT:** The daunting energy challenges in the 21st century are a result of over-reliance on limited fossil fuels coupled with ever-increasing energy demand. Among the solutions is the development of technologies and infrastructures to help in the smooth transition to alternative and renewable energy sources. Nanotechnology, a combination of chemistry and engineering, is viewed as the new candidate for clean energy applications. It involves the manipulation of nanoscale structures to integrate them into larger material components and systems. In comparison to bulk materials, nanomaterials have high surface areas and are expected to exhibit higher activities. They also demonstrate better stability and durability and are more cost-effective with high recycling potential. This paper reviews selected recent advances in the development of nanotechnology in the emerging solar energy and biofuel fields. Special emphases are given to studies on photovoltaics (including Schottky junction solar cells, organic solar cells, quantum dot-sensitized solar cells, and earth-abundant $Cu_2ZnSnS_4$ materials) and artificial photosynthesis. As for the biofuel section, a review on the use of nanotechnology in transesterification, gasification, pyrolysis, and hydrogenation, as well as in the reforming of biomass-derived compounds is given. As these technologies become more mature, efficient, and economical, they could eventually replace traditional fossil fuels.

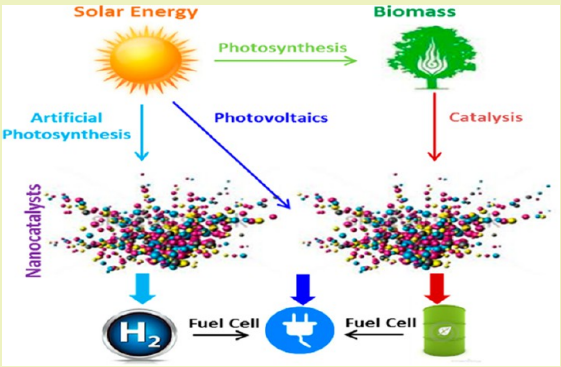


**KEYWORDS:** *Nanotechnology, Nanoparticles, Biofuels, Solar energy, Photovoltaics, Hydrogen*

## INTRODUCTION: NANOTECHNOLOGY IN THE ENERGY SECTOR

One of the biggest challenges for mankind in this century is to secure a long-term energy supply for sustainable global development.[1] We are increasingly dependent on fossil fuels, our current energy source. Furthermore, the combustion of these fuels causes environmental degradation through air pollution and global warming. Though it will take some decades to come close to a truly sustainable energy system, intensive research is being conducted to find solutions to (1) increase efficiency in production, transmission, and utilization of the remaining fossil fuels, (2) reduce negative impacts to the environment, and (3) develop or improve technologies and infrastructure for the smooth transition to the alternative/renewable energy sources (e.g., nuclear power, solar energy, wind power, geothermal energy, biomass and biofuels, and hydropower).[2] Nanotechnology, the control of materials and phenomena at scales between 1 and 100 nm, holds the key to many of the technological advancements in the energy sector. It involves the miniaturization as well as the manipulation of atoms and molecules to control their properties, which at this scale are so different from the bulk properties. For instance, a 100 nm particle has less than 0.2% of atoms on the surface, while a 10 nm particle has about 10% on the surface and a 2 nm particle has 90% of its atoms on the surface. Because these surface atoms may have more than one dangling bonds, they are very active and tend to form bonds with adjacent molecules to become more stable. This translates into more chemical activity, lower melting point, and higher solubility.[3] Nanomaterials have been and are being studied for various renewable energy applications. Figure 1 shows the potential applications of nanotechnology in some key energy processes.

This review focuses on the use of nanotechnology in two major energy fields: solar energy, with an emphasis on photovoltaic (PV) solar cells and artificial photosynthesis, and biofuels, including transesterification, gasification and pyrolysis, hydrogenation and reforming. The aim of this review is an attempt to examine the role of nanotechnology in solar and biofuels and spike the attention of the reader on these current research topics.

## SOLAR FUELS

The available supply of solar energy is about 15,000 fold greater than the combined energy derived every year from nuclear and fossil fuels for consumption. The potentially usable solar energy at the insolation of 10 kW/m$^2$ or greater is about $3.9 \times 10^{24}$ J/yr.[4] Sunlight is diffuse and intermittent, and in order to use this free energy for humanity needs, energy storage in dense transportable media will be required.[5] This section will focus on nanotechnology use in energy-related processes that involve solar radiation as an energy source and in particular in photovoltaics and artificial photosynthesis. Different technolo-

**Special Issue:** Sustainable Nanotechnology

**Received:** February 15, 2013
**Revised:** May 20, 2013
**Published:** May 22, 2013

ACS Publications © 2013 American Chemical Society

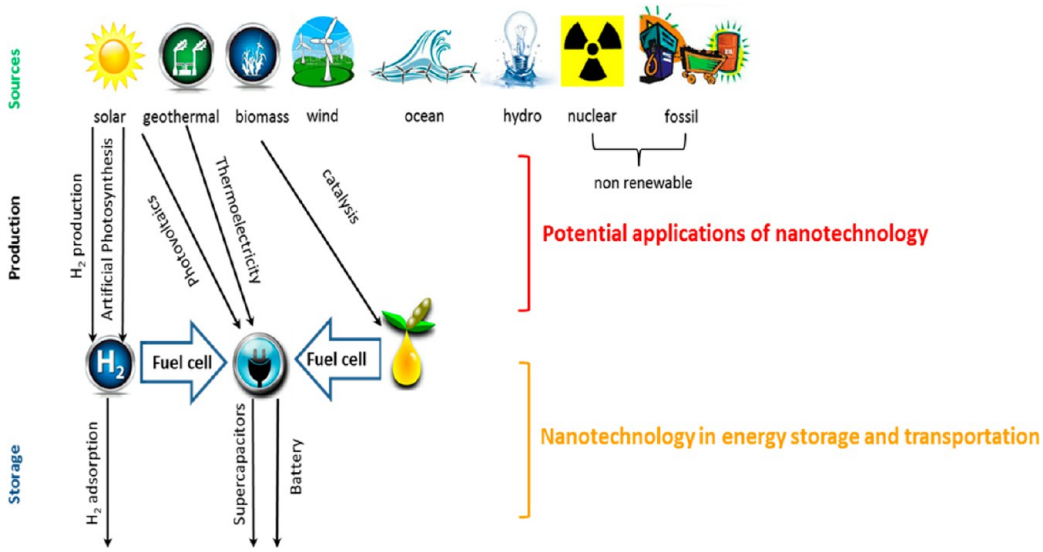


**Figure 1.** Most promising applications of nanotechnology for the energy production domain (adapted from ref 2).

gies have been used to harness solar energy, including photovoltaic technology and solar−thermal systems (solar collectors, artificial photosynthesis). Nanoscience researchers are currently working on improving the photosynthesis efficiency with the goal that artificial photosynthesis could create hydrogen for industrial storage, assist crop production on marginal lands, and reduce atmospheric $CO_2$ among others.[4] The use of nanotechnology to make inexpensive and efficient solar cells on a large scale is also of great promise. In particular, nanostructured layers in thin-film solar cells offer three important advantages: (i) because of multiple internal reflections, the effective optical path for absorption is much larger than the actual film thickness, (ii) light generated electrons and holes need to travel over a much shorter path, and thus recombination losses are greatly reduced, and (iii) the energy bandgap of various layers can be tailored to match the radiation by varying the size of the nanoparticles (NPs). This allows for a good design flexibility in the absorber and window layers in the solar cell.[6]

Throughout this review and the referred literature, several kinds of conversion efficiencies are reported. In order to help the readers, a brief definition of these efficiencies is given. A solar cell can be operated over a wide range of voltages ($V$) and current ($I$) to determine the maximum power point at which the cell delivers maximum electrical power. This can be achieved by continuously applying voltage on an irradiated cell from $V = 0$ through the point $I = 0$ to a very high value of $V$. The ***power conversion efficiency***[7] ($\eta$), defined as the percentage of the solar power that is converted from absorbed light to electrical energy, is estimated, using the following equation

$$\eta = \frac{V_{oc} I_{sc} \mathrm{FF}}{P_{in}}$$

where $V_{oc}$ is the open circuit voltage (when no current passes through the cell), $I_{sc}$ is the short circuit current (when voltage is zero), FF is the fill factor (a measure of the "squareness" of the $I-V$ curve), and $P_{in}$ is the input light irradiance, which illuminates the cell. The efficiency depends on the spectrum and intensity of the incident sunlight and the temperature of the solar cell. Therefore, conditions under which efficiency is measured must be carefully controlled in order to compare the performance of one device to another. Terrestrial solar cells are measured under AM1.5 conditions and at a temperature of 25 °C. Solar cells intended for space use are measured under AM0 conditions.

The photovoltaic response of a solar cell to monochromatic light is measured to calculate how efficiently the cell converts photons of a given wavelength into electrons. An ***external quantum efficiency*** (**EQE**) or ***incident photon (to charge) conversion efficiency*** (**IPCE**) value is most often expressed as the percentage of incident photons that are absorbed and converted into electrons by the solar cell as a function of wavelength. If the absorption spectrum of the solar cell is known, the fraction of absorbed photons can be used to calculate the ***internal quantum efficiency*** (**IQE**). This value gives the percentage of photons absorbed by the cell that are converted into electrons as a function of wavelength. In this review, some of the experiments make use of an IPCE monochromator that provides light of very narrow bandwidth (nearly monochromatic). By measuring the power at each wavelength, the number of photons that are generated can be calculated. If this light is incident on a solar cell, the output current generated by the solar cell (with zero bias voltage) can be used to calculate the number of electrons that are generated. This measurement provides information about how efficiently a cell converts photons of a particular frequency into electrons. Unlike an AM1.5 power conversion efficiency measurement, an IPCE measurement does not indicate the total power efficiency of the cell. This is because the total output power of the solar cell depends on the operating voltage of the cell, and IPCE values are measured with the cell in short circuit conditions.

Careful measurement of the power at a given wavelength can be used to calculate the number of photons that are incident on the solar cell through the following equation

$$\frac{\#\mathrm{photons}}{s} = \frac{P_{in}}{hf} = \frac{P\lambda}{hc}$$

where $h$ is Plank's constant ($6.626068 \times 10^{-34}$ m$^2$ kg/s), $c$ is the speed of light (299 792 458 m/s), $\lambda$ is the wavelength in meters, and $P_{in}$ is the power incident on the cell, in watts. When a cell is under illumination, the number of generated electrons can easily be calculated by measuring the output current of the

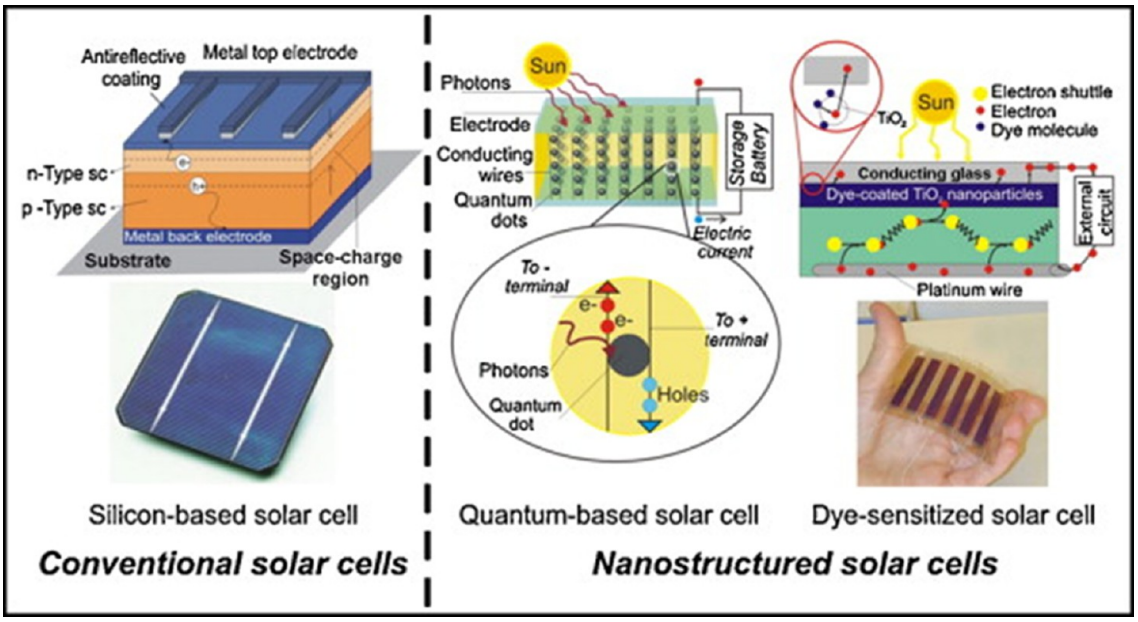


**Figure 2.** PV technology evolution from conventional to nanostructured solar cells (reproduced with permission from Elsevier Science).[11]

cell under short circuit conditions ($V_{bias}$ = 0) and using the following equation

$$\frac{\#\text{electrons}}{s} = \frac{I_{sc}}{e}$$

where $I_{sc}$ is the short circuit current, and e is the charge of an electron ($1.602 \times 10^{-19}$ C). Calculating the EQE is then simply

$$\begin{aligned}\text{EQE}(\%)|_\lambda &= \left.\frac{\#\text{electrons}}{\#\text{photons}} \times 100\right|_\lambda \\ &= \left.\left(\frac{I_{sc}/e}{P/(hf)}\right)\right|_\lambda \\ &= \left.\left(\frac{I_{sc}/e}{P\lambda/(hc)}\right)\right|_\lambda \\ &= \left.\left(\frac{hc}{e}\right)\left(\frac{I_{sc}}{P\lambda}\right)\right|_\lambda\end{aligned}$$

where the value of the incident power and current need to be measured at each wavelength.[8]

## ■ PHOTOVOLTAICS

Sunlight is composed of photons, or particles of solar energy. These photons contain various amounts of energy corresponding to the different wavelengths of the solar spectrum. When light strikes a PV cell (usually a semiconductor like Si), it may be reflected, absorbed, or may go right through. Only the absorbed photons generate electricity. When such light strikes a bound electron in the semiconductor, the electron "escapes" from its place in the crystal. This leaves behind a bond missing an electron (a hole) and a free electron moving about in the crystal (the mobile electron−hole pairs are referred to as "excitons"). The free electron is said to be in the crystal's conduction band because free electrons are a means by which electricity flows. To produce an electric force and current, a mechanism is needed to avoid having the electrons and holes rejoin and lose their electrical properties. Doping, a process through which impurities are introduced into a pure semiconductor, is one of the mechanisms to obtain "n" and "p" type semiconductors. The "p" and "n" type of semiconductors correspond to "positive" and "negative" because of their abundance of holes or electrons (extra electrons make a "n" type because electrons are negatively charged). Therefore, n-type silicon (doped with, for example, phosphorus) has excess electrons, and p-type silicon (doped with, for example, boron) has excess holes. Sandwiching these together creates a p/n junction at their interface, thereby creating an electric field.[9]

There are basically three generations of PV technologies. The first generation was built on high-quality single crystalline silicon wafers giving a high efficiency (∼15%) but at a high production cost. The second generation is represented by thin-film devices based on cadmium telluride (CdTe), copper indium gallium selenide (CIGS), and amorphous silicon. They have lower energy and production costs but suffer from much reduced conversion efficiencies. The third generation aims to increase the efficiency of the second generation solar cells, while maintaining low production costs (Figure 2).[2] The solar cells used presently have photons with energies greater than the semiconductor bandgap (energy difference between the states in which the electron is bound to the atom and when it is free to conduct throughout the crystal), creating free carriers or excitons. This kinetic free energy is lost quickly through electron−phonon scattering or through conversion to heat. These excitons then occupy the lowest energy levels and can be removed though electrical/chemical work or radiative/non-radiative recombination. In order to reduce the energy loss due to carrier cooling, staking of a series of semiconductors, use of hot carriers, or quantum dots have been contemplated.[10] Nanostructured semiconducting materials hold the promise of achieving high efficiency at low cost. Nanotubes and quantum dots are being actively studied in order to improve the conversion efficiency of the PV cells by controlling the energy bandgap and enhancing the effective optical path.

Research in this area aims at boosting the solar-to-electrical energy conversion efficiency beyond the traditional Shockley and Queisser limit of 32% for a single junction photovoltaic

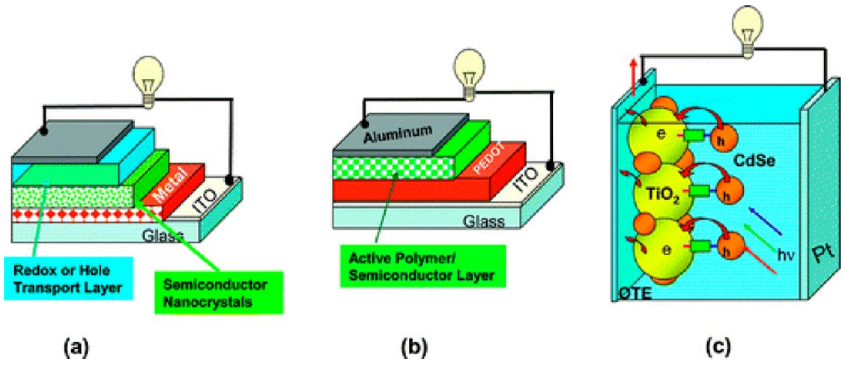


**Figure 3.** Development of quantum dot-based solar cells: (a) metal–semiconductor junction, (b) polymer–semiconductor, and (c) semiconductor–semiconductor systems (reproduced with permission from the American Chemical Society).[12]

cell. In this quest, three types of solar cells, exploiting the properties of semiconductor nanocrystals (quantum dots), have emerged: (a) metal-semiconductor or Schottky junction photovoltaic cell, (b) semiconductor nanostructure–polymer solar cell, and (c) semiconductor sensitized quantum dot solar cell (Figure 3).[12]

Quantum Dots (QDs) are semiconducting nanometer crystals, fabricated in different forms to obtain tunable bandgap of energy levels that allow them to behave as special semiconductors. They are composed of periodic groups of II–VI, III–V, or IV–VI materials. QDs can better match the solar spectrum because their absorption spectrum can be tuned with the particle size (for example, larger quantum dots emit or absorb longer wavelengths of the solar spectrum).[13] With a greater semiconductor bandgap, a solar cell absorbs more energetic photons generating a greater output voltage. On the other hand, with a lower bandgap, the cell will capture more photons resulting in higher output current but lower output voltage. With semiconductor quantum dots, there are two ways to increase the photon conversion efficiency: production of multiple excitons from a single photon of sufficient energy and the formation of intermediate bands in the bandgap that use sub-bandgap photons to form separable electron–hole pairs.[14]

**Semiconductor–Metal (or Schottky) Junction Solar Cell.** A photovoltaic cell can be created from the Schottky junction between a semiconductor and a metal, with or without an insulating layer between them. These types of solar cells date back to 1883 when Charles Fritts coated selenium with a thin layer of gold. An interface between a metal and semiconductor can induce a depletion or inversion layer in the semiconductor. A built-in potential called the "Schottky barrier" appears between the bulk of the semiconductor and the surface. Usually, the metal is deposited as a semi-transparent film through which most of the light can pass.[7] In the case of QDs, they are spin-cast from solution, leading to smooth densely packed arrays. When light hits the PV cell, a small amount can be absorbed in the metal and excites the electrons over the metal into the semiconductor. Light transmitted through the metal into the semiconductor is mainly absorbed in the depletion region, creating electron–hole pairs. Longer wavelength light is absorbed in the neutral regions, and the holes diffuse to the depletion edge to be collected.

According to the classical theories, p-type and n-type doping of an intrinsic material introduces new energy levels in the bandgap close to the band edges. This changes the chemical potential of electrons in the material (the work function) as described by the Fermi level.[15] When a semiconductor comes into contact with a metal surface, it also undergoes Fermi level (electrochemical potential) thermal equilibration by building up space–charge layers at the interface because the materials have different work functions. In a PV cell, when the semiconductor–metal junction is subjected to bandgap excitation, the band bending rectifies the photogenerated charge carriers' flow to produce a current in the solar cell. When semiconductor nanocrystals are used, the electrons are confined, and the individual nanocrystals remain isoenergetic. The bands remain flat, and charge separation is dictated by the Fermi level equilibration. With different electron accumulation degrees, the nanocrystal can attain different Fermi levels, creating an energy gradient to drive the electrons toward the electrode. If both the metal and semiconductor QDs are in a particulate form, there will be electron storage within the particles.[12] For example, studies have shown that Au nanoparticles (NPs) store electrons in a quantized fashion. Nanometer-sized monolayer-protected gold clusters were anchored to macroscopic gold electrodes to give double-layer charging that facilitated electron storage.[16] This electron accumulation increases the Fermi level of the metal to more negative potentials, shifting the resultant Fermi level of the composite closer to the conduction band of the semiconductor. This phenomenon (Figure 4) has also been observed in the

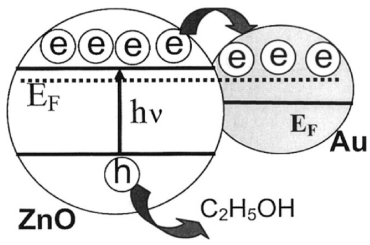


**Figure 4.** Fermi level equilibration: charge distribution in semiconductor–metal composite system (reproduced with permission from the American Chemical Society).[18]

case of $TiO_2$/Au[17] and ZnO/Au.[18] The Au NPs capped with organic molecules have unusual redox activity such that when they come into contact with a charged semiconductor nanoparticle they readily accept electrons and undergo Fermi level equilibration. Studies[19] have also looked into attaching nanometer-sized insulating quantum dots (CdS, CdSe, and ZnO) to the Au substrate, using molecular bridges with thiol and carboxylate end functions. In the case of CdS, the NP keeps its size and semiconducting properties even after being

immobilized on the substrate.[19a] Charge injection and transport have also been investigated in thin disordered films of CdSe nanocrystals between metal electrodes. It was found that high work function materials such as gold and indium−tin oxide are poor electron injectors and that their conductivity is strongly temperature dependent.

These observations were consistent with the estimated conduction and valence band levels of the nanocrystals.[20] *p*-Aminothiophenol-capped CdS nanoparticles (8.5 ± 0.3 nm in size), assembled as a monolayer on Au electrode, were observed to have efficient photoelectrochemical properties in the presence of triethanolamine as sacrificial electron donor and acted as a tunneling medium for transporting the electrons from the semiconductor nanoparticles to the electrode.[21] Visible light nanoscale photocatalysis was used with highly controlled hybrid gold-tipped CdSe nanorods (nanodumbbells). Under visible light irradiation, charge separation takes place between the semiconductor and metal parts of the hybrid particles, followed by direct photoreduction of a model acceptor molecule, methylene blue.[22] An example of nanostructured layers in thin-film solar cells has been reported by one study whereby nanocrystalline CdTe and nanostructured CdS films in crystalline, porous, and fiber forms were deposited on indium tin oxide (ITO)-coated glass substrates. CdTe nanocrystals of 10 nm had an effective bandgap of 2.8 eV, while 15 nm CdS nanocrystals had an effective bandgap of 2.98 eV. The porous CdS and $TiO_2$ films were deposited on plastic substrates by a self-assembly method with typical pore sizes of 80 and 70 nm, respectively. These can be used in nanostructured solar cell configuration where the pores are filled with a suitable absorber material. The typical particle size of $TiO_2$ nanocrystalline films was 10 nm, while the CdS fibers were 80 nm wide and 1.5 $\mu$m long.[6]

Even if the Schottky junction-based QD solar cells are not yet fully developed, recent findings are showing promise. Recent advances in colloidal quantum dot (CQD) photovoltaics have led to impressive 3.6% solar power conversion efficiencies under simulated 99.8 mW/cm$^2$ AM1.5G (i.e., air mass coefficient 1.5 global) solar illumination.[23] One study used two distinct device architectures and operating mechanisms: (i) the Schottky device was optimized and explained in terms of a depletion region driving electron−hole pair separation on the semiconductor side of a junction between an opaque low-work-function metal and a p-type CQD film and (ii) the excitonic device that employed a CQD layer atop a transparent conductive oxide (TCO) was explained in terms of diffusive exciton transport via energy transfer followed by exciton separation at the heterointerface between the CQD film and the TCO.[24] The CQD photovoltaic devices were fabricated on TCOs, and the resultant depleted heterojunction solar cells provided a 5.1% AM1.5 power conversion efficiency. The solar spectrum at AM1.5 was simulated to within class A specifications (less than 25% spectral mismatch) with a Xe lamp and filters (Solar Light Company, Inc.) with measured intensity at 94 mW cm$^{-2}$. A recent study done at the National Renewable Energy Laboratory looked into the multiple exciton generation (MEG), a process occurring in QDs, whereby absorption of a photon bearing at least twice the bandgap energy produces two or more electron−hole pairs. A photocurrent enhancement arising from MEG in lead selenide (PbSe) QD-based solar cells was reported. The hydrazine treatment allowed multiple carriers produced by MEG to be efficiently collected in a solar cell made from electronically coupled QDs. The maximum external quantum efficiency (spectrally resolved ratio of collected charge carriers to incident photons) was 114 ± 1% with an associated internal quantum efficiency (corrected for reflection and absorption losses) of 130%. It was concluded that MEG charge carriers can be collected in suitably designed QD solar cells, encouraging more research to enhance the efficiency of solar light-harvesting technologies.[25]

**Organic Solar Cell.** During the last three decades, much effort has been dedicated to developing organic solar cells. Semiconducting organic materials can transport electric current and absorb light in the ultraviolet spectrum due to the $sp^2$-hybridization of carbon atoms. For example, conducting polymers have $sp^2$-hybridized carbon atoms that each have an electron in the $p_z$ orbital. These electrons will form Π-bonds with neighboring $p_z$ electrons in a linear chain of $sp^2$-hybridized carbon atoms. This leads to dimerization through the formation of alternating single and double bond structures. Because of the isomeric effect, these Π-electrons are of a delocalized nature, resulting in high electronic polarizability. Furthermore, organic semiconductors have relatively strong absorption coefficients ($\geq 10^5$ cm$^{-1}$), which balance low mobilities and give high absorption in thin devices. Even though organic semiconductors are hole conductors and have a higher optical band compared to silicon (thus limiting solar spectrum harvest), they exhibit chemical flexibility for modifications and have low cost.[26] Usually, bicontinuous blends of two organic semiconductor materials, most often a conjugated polymer (electron donor) blended with a $C_{60}$ derivative (electron acceptor), are used for the photoactive layer to form a bulk heterojunction. With optical excitation, photoinduced charge separation occurs with charge transport through the two phases resulting in a current output to an external circuit. Usually, the polymer poly(3-hexylthiophene) (P3HT) and the $C_{60}$ derivative, PCBM ([6,6]-phenyl-C61-butyric acid methyl ester) are used.[12,27] Solar cell efficiencies in excess of 4% were obtained with this combination of organic materials under the standard AM1.5G 1 sun test condition.[28] The high efficiency obtained is due to the properties of this unique combination of materials. The treatment procedure dictates the morphology of the heterogeneous junction, which is critical for power conversion efficiency (PCE) optimization. In one study, it was observed that in the case of P3HT and PCB, both blend morphology and photovoltaic device performance are influenced by the treatment conditions used including choice of solvent, rate of drying, and type of annealing (thermal or vapor). On the basis of the observations, a morphology evolution consisting of an initial crystallization of P3HT chains, followed by diffusion of PCBM molecules to nucleation sites, at which aggregates of PCBM then grow, was then proposed.[29] The lifetime of these flexible organic solar cells (P3HT:PCBM bulk heterojunctions) was investigated under laboratory (1 sun illumination at 65 °C in order to accelerate the degradation) and outdoor conditions (at the Konarka rooftop testing setup in Lowell, MA, U.S.A.). It was seen that the polymer solar cells have a good light stability, passing 1000 h under accelerated light-soaking conditions in the laboratory, and they survived over 1 year of outdoor exposure without performance losses.[30] The relation between the open circuit voltage ($V_{oc}$) and the oxidation potential for different conjugated polymers was studied for the photovoltaic cells made from conjugated polymers and a fullerene derivate. A linear relation between $V_{oc}$ and the oxidation potential was found so that the energy

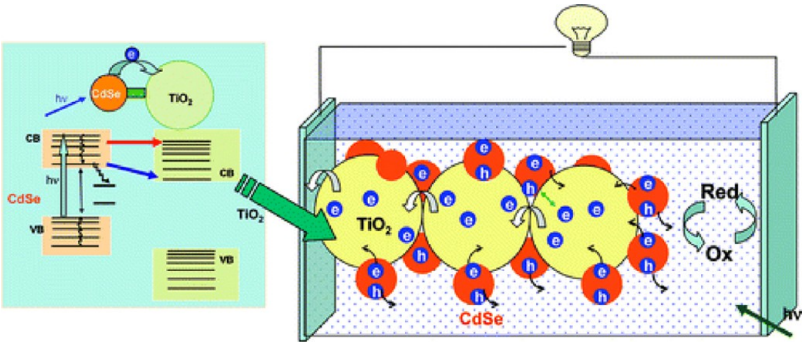


**Figure 5.** Principle of operation of quantum dot-sensitized solar cell (QDSSC) (reproduced with permission from the American Chemical Society).[12]

conversion efficiency of a bulk heterojunction solar cell could be derived as a function of the bandgap and the energy levels of the conjugated polymer. This model could also be used as a guideline to select materials for the solar cells.[31]

To improve the efficiency of the P3HT:PCBM system, new materials would be needed because this state-of-the art solar cell has approached its optimal performance. The bandgap of P3HT is around 1.9 eV, while the photon flux from the sun reaching the earth has a maximum of 1.8 eV. Only 22.4% of the solar photons are actually harvested, and a lower bandgap of the active material is desirable to increase the efficiency. One way to synthesize low bandgap polymers is the donor−acceptor approach by alternating electron-rich and electron-poor units in the polymer backbone. Poly[2,6-(4,4-bis-(2-ethylhexyl)-4H-cyclopenta[2,1-b;3,4-b′]-dithiophene)-alt-4,7-(2,1,3-benzothiadiazole)] (PCPDTBT) has both an acceptor and donor unit with an optical bandgap of 1.46 eV. Using bulk heterojunction solar cells based on PCPDTBT and [70]PCBM, power conversion efficiencies of up to 3.5% and an external quantum efficiency of at least 25% between 400 and 800 nm (with a maximum of 38% around 700 nm) were obtained. Device characterization was carried out under AM1.5G irradiation (100 mW/cm$^2$) on a xenon solar simulator with a spectral mismatch of 0.83 for the spectral range down to 1000 nm.[32] By incorporating a few vol % of alkanedithiols in the solution used to spin-cast films comprised of a low-bandgap polymer and a fullerene derivative, the PCE of photovoltaic cells increased from 2.8% to 5.5% due to alteration of bulk heterojunction morphology. The efficiencies were measured using a 150W AM1.5G light source operating at 80 mW cm$^{-2}$ as well as an independent 300W AM1.5G source operating at 100 mW cm$^{-2}$ for cross-checking the results.[33] A power conversion efficiency of 6% was obtained from an alternating copolymer, PCDTBT in bulk heterojunction composites with the fullerene derivative [6,6]-phenyl $C_{70}$-butyric acid methyl ester ($PC_{70}BM$). These solar cells exhibit the best performance of any bulk heterojunction system studied to date, under an air mass 1.5 global (AM1.5G) solar simulator with an irradiation intensity of 1000 W m$^{-2}$. The spectral mismatch factor was calculated by comparing the spectrum of the solar simulator with that of the AM1.5 spectrum at room temperature. Because the internal quantum efficiency was nearly 100%, every absorbed photon resulted in a separated pair of charge carriers and all photogenerated carriers were collected at the electrodes.[34] Organic semiconductors may play a major role in microelectronics in the future. Combinations of these solar cells with batteries, fuel cells, etc. will improve their integration into many products.

**Quantum Dot-Sensitized Solar Cells (QDSSC).** Quantum dot-sensitized solar cells (QDSSC) are based on ensembles of nanometer-sized heterointerfaces between two semiconducting nanostructured materials. Short bandgap semiconductor quantum dots such as CdSe, InP, PbS, and PbSe have tunable band edges and can be used to harvest light in the visible light region.[12] In these cells, QDs are attached to a wide bandgap material (such as $TiO_2$ or ZnO) via a linker with bifunctional molecules of the form X−R−Y (where X and Y are functional groups, such as carboxylic, thiol etc., and R is an alkyl group). Sometimes, QDs are directly attached to the wide bandgap material without a linker molecule. A thin layer of liquid electrolyte containing a redox couple or a hole conductor is sandwiched between this photoelectrode and a counter electrode. The QDs absorb the incident photons to form photoexcited electron−hole pairs that are confined within the nanocrystal. The device configuration separates the positive and negative photogenerated carriers into different regions of the solar cell to avoid recombination. Figure 5 illustrates the principle of operation of a QDSSC. In this configuration, QDs are chemisorbed onto the surface of 10−30 nm $TiO_2$ particles that have been sintered into a highly porous nanocrystalline 10−20 $\mu$m $TiO_2$ film. As the QDs are photoexcited, the electrons are injected from the excited state of the QDs into the conduction band of the semiconductor, $TiO_2$, affecting charge separation and producing a photovoltaic effect.[14] The redox electrolyte (e.g., sulfide/polysulfide) scavenges the holes and thus ensures regeneration of the CdSe.

One group fabricated planar D−A (donor−acceptor) heterojunctions by sequentially spin-casting films of CdTe and then CdSe on indium tin oxide (ITO) glass coated with alumina to form an ultrathin donor−acceptor solar cell. These devices are stable in air, and post-fabrication processing allows for external quantum efficiencies of 70% and power conversion efficiencies approaching 3% in the initial tests under simulated AM1.5G illumination. Because of the tunneling of the charge carriers through the thin organic layer between CdTe and CdSe nanocrystals, there is a spatial charge separation of the photoexcited electron−hole pairs leading to an efficient quenching of photoluminescence.[35] Some studies have assembled semiconductor nanoparticles using bifunctional surface modifiers of the type HS−R−COOH for use in photoelectrochemical cells. In a typical procedure, the optically transparent electrode modified with $TiO_2$ particulate film is immersed in an acetonitrile solution of HCOOC−R−SH for 2−4 h. The electrode is then immersed in a toluene suspension of CdSe QDs after washing with acetonitrile. $TiO_2$ has a strong affinity for the carboxylate group, while CdSe will bind to thiol

and amine groups. Upon visible light excitation, CdSe QDs inject electrons into $TiO_2$ nanocrystallites, and these charge carriers can then be collected at a conducting electrode to generate a photocurrent. Photocurrent and photovoltage were measured using a programmable electrometer along with collimated filtered light from a 450 W xenon arc lamp. A high-intensity grating monochromator was also introduced into the light path to select the excitation wavelength during measurements. A photon-to-charge carrier generation efficiency of 12% was obtained with the $TiO_2$−CdSe composite when employed as a photoanode in a photoelectrochemical cell.[36]

Another approach to increasing energy harvesting in $TiO_2$-based photoelectrochemical solar (PES) cells is based on photonic crystals and photonic sponge new architectures. It was observed that better photoelectrical performances were obtained when the $TiO_2$ electrode was structured to localize photons. The efficiency of the dye-sensitized PES cells increased because of the photonic sponge topology.[37] The effect of neighboring metal nanoparticles on photovoltaic and photocatalytic behavior of semiconductor nanostructures was also studied. It was found that the performance of dye-sensitized solar cells (DSSC) is influenced by the neighboring metal nanoparticles. For example, the efficiency (9.3%) of an N719 dye-sensitized solar cell increased to 10.2% upon incorporation of 0.7% Au/$SiO_2$ and to 9.8% upon loading of 0.7% Au/$TiO_2$ nanoparticles. The experiments were conducted by photolyzing a $N_2$-purged solution with UV−visible light (250 W xenon lamp). A $CuSO_4$ filter was introduced in the path of the light beam to cut off light below the wavelength of 300 nm.[38] Synthesized $Ti_{1-x}Sn_xO_2$ nanoparticles were used to prepare $TiO_2$ nanotubes that were adapted to the photoelectrodes of DSSCs. A high overall conversion cell efficiency of 6% was achieved by nanotube photoanodes synthesized from 5% $SnO_2$-doped $TiO_2$ nanoparticles (superior to electrodes prepared by both Sn-doped and nondoped $TiO_2$ NPs and pure $TiO_2$ nanotubes). A solar simulator (Oriel Sol 3ATM) with a Keithley 2400 source meter under AM1.5G illumination condition (100 mW/cm$^2$) was used for all measurements. $TiO_2$ nanotube electrodes showed enhanced photovoltaic performance, which may be attributed to the formation of an appropriate defect in the oxide photoelectrode films.[39] It is noted that for all the QD solar cells, the most important parameter for reaching very high conversion efficiency is the multiple electron−hole pair production in the photoexcited QDs. It is critical to capitalize on research geared toward this end.

**Earth Abundant $Cu_2ZnSnS_4$ (CZTS).** For sustainable photovoltaic solar cells, the materials have to give high energy conversion efficiency and be nontoxic and earth abundant. It is challenging to obtain all the desirable properties in a single material because sometimes high-efficiency devices may very often contain toxic elements, or green materials may not always give best device performance. New materials like earth-abundant $Cu_2ZnSnS_4$ (CZTS) have emerged as a promising absorber for thin-film solar cells.[40] CZTS is composed of earth-abundant materials that have low cost and toxicity and can be sustainable for the fabrication of thin-film solar cells. Compared to two high-efficiency thin-film solar cells with CdTe and $Cu(In_{1-x},Ga_x)S_2$ (CIGS) that have toxic elements (Cd) and rare metals (indium and gallium), respectively, CZTS is environmentally friendly. PV performance of CZTS as a p-type semiconductor has been demonstrated owing to its direct bandgap of 1.5 eV and a large absorption coefficient (>$10^4$ cm$^{-1}$).[41] One study has also used CZTS in DSSCs. A PCE of 7.4% was achieved by a simple process of spin-coating CZTS followed by selenization. A solar simulator was used to simulate sunlight for an illumination intensity of 100 mW cm$^{-2}$. This efficiency was highly comparable to the DSSC prepared by utilizing Pt with a power conversion efficiency of 7% under a similar device configuration.[42] A number of techniques have been used to fabricate CZTS, among which is colloidal synthesis. The CZTS nanocrystals were made by high-temperature arrested precipitation in a coordinating solvent, oleylamine (OLA). Copper(II) acetylacetonate [$Cu(acac)_2$], zinc acetate [$Zn(O_2CCH_3)_2$], tin(II) chloride dihydrate [$SnCl_2{\cdot}2H_2O$], and elemental sulfur (S) were combined in OLA and heated to 280 °C for 1 h under an inert atmosphere. The transmission electron microscopy (TEM) and scanning electron microscopy (SEM) images of the so-prepared CZTS nanocrystals show an average diameter of 10.6 ± 2.9 nm (Figure 6).[43]

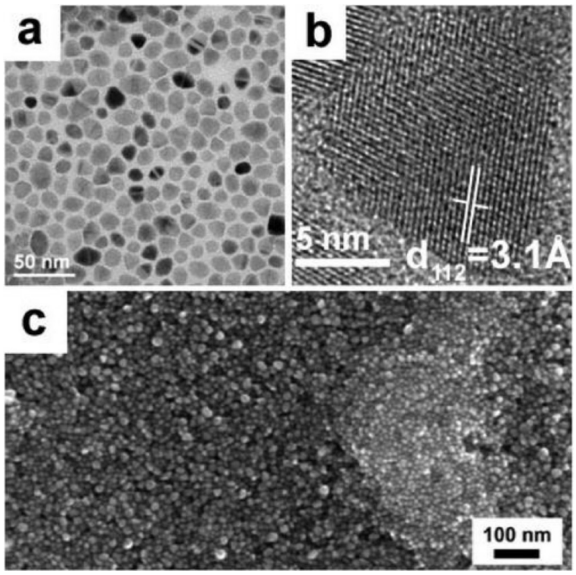


**Figure 6.** (a, b) TEM and (c) SEM images of CZTS nanocrystals (reproduced with permission from the American Chemical Society).[43]

One study looked at the selenization of CZTS nanocrystals to form CZTSSe (copper−zinc−tin−chalcogenide). It was found that tuning the composition of the CZTS nanocrystals and developing a robust film coating method, a total area efficiency as high as 7.2% under AM1.5 illumination after light soaking for 15 min under one sun illumination could be achieved. However, the change in device performance is temporary, and PCE goes back down to its starting point (6.98%) after the light is turned off.[44] The same group then synthesized $Cu_2Zn(Sn_{1-x}Ge_x)S_4$ nanocrystals in oleylamine with no additional surfactants to be used as the photoabsorbing layer in a thin-film solar cell. The adjustment of the Ge/(Ge+Sn) ratio of the nanocrystal synthesis precursors dictates the bandgaps of the nanocrystals. For example, the solar cells from $Cu_2ZnGeS_4$ nanocrystal films yielded a PCE of 0.51%, while $Cu_2Zn(Sn_xGe_{1-x})S_4$ nanocrystals with a Ge/(Ge+Sn) ratio of 0.7 yielded devices with an efficiency of 6.8%. Hence, Ge gradients can be formed to direct minority carriers away from high recombination interfaces and significantly improve the device efficiency of CZTSSe-based solar cells.[45]

A recent paper demonstrated a power conversion efficiency record of 10.1% using kesterite absorbers, with a $Cu_2ZnSn(Se,S)_4$ thin-film solar cell made by hydrazine-based solution processing. A solar simulator equipped with a closed-loop light stabilization system was used for electrical characterization under simulated air mass 1.5 global (AM1.5G) spectrum. A Protoflex system equipped with a xenon light source and a monochromator was utilized to measure the quantum efficiency. The record kesterite device was shown to be primarily limited by interface recombination, minority carrier lifetime, and series resistance. If shortcomings of this device are addressed, CZTSSe would be able to achieve further performance gains and join CdTe as a commercially viable high-performance solar cell technology.[46]

## ■ ARTIFICIAL PHOTOSYNTHESIS

Natural photosynthesis is the largest-scale best-tested method for solar energy harvesting on the planet, but the efficiency of photosynthetic conversion of sunlight to stored energy in forms useful to humans is rather low.[5] Inspired by natural photosynthesis, low-cost and environmentally friendly hydrogen production based on the use of solar energy through photocatalytic water splitting into hydrogen and oxygen (termed as artificial photosynthesis) is currently under intensive research where nanomaterials help to increase the efficiency of hydrogen production. Under solar radiation, semiconductor materials can help in splitting water into hydrogen and oxygen. A semiconductor consists of valence band (VB) and conduction band (CB). The energy difference between these two levels is termed the bandgap. Both the electrons and holes are in the valence band, but when excited by photons with energy equal to or higher than their bandgap energy level, these electrons receive energy from the photons. They are thus promoted from VB to CB if the energy gain is higher than the bandgap energy level. These photogenerated electrons and holes can either recombine in bulk or on the surface of the semiconductor or migrate to the surface of the semiconductor. When they migrate, the electrons and holes can reduce and oxidize reactants adsorbed by the semiconductor. An example of a reduction reaction is the photocatalytic production of hydrogen.[47] Details of the principles of photocatalytic hydrogen generation can be found in the review by Mao et al.[3,48]

Thermodynamically, the overall water splitting reaction is an uphill reaction with a highly positive change in Gibbs free energy [$\Delta G^0 = +237.2$ kJ mol$^{-1}$: $H_2O(l) \rightarrow H_2(g) + 0.5O_2(g)$]. Hydrogen can serve as an excellent energy carrier, provide higher energy conversion efficiency than current fossil fuel internal combustion engines, and does not generate $CO_2$ or other pollutants. Photoelectrochemical (PEC) hydrogen generation from water splitting has been validated by successful demonstration using PEC cells, but the efficiency of these devices have been limited due to low light absorption efficiency and the recombination of photoexcited electrons and holes.[49] $TiO_2$-based artificial photosynthesis has been used because this semiconductor is highly stable over a wide range of pH values, is abundant and nontoxic, and has strong catalytic activity. However, it absorbs less than 12% of the incident sunlight due to its large bandgap. Because of their high surface areas, nanosized semiconductors are now being investigated because they would in principle allow faster charge capture by the solution species and lower probability of bulk charge recombination.

In 1997, a study[50] demonstrated long-lived charge separation in a nanostructured $TiO_2$ membrane for water splitting on nanostructures. Later, studies by Khan et al. showed the photoresponse of nanocrystalline n-$TiO_2$, n-$TiO_2$/$Mn_2O_3$, and n-$Fe_2O_3$ thin-film electrodes for water splitting.[51] The $Mn_2O_3$ deposition enhanced the oxygen evolution and improved the stability of the n-$TiO_2$ film electrodes, while the n-$Fe_2O_3$ films exhibited higher photoresponse when compared to the powdered or iron sheet forms. Therefore, high-quality nanostructures are required to improve the efficiency of the water splitting reaction, which led to the development of a hybrid multi-junction photoelectrode consisting of amorphous silicon/germanium and iron oxide thin films.[52] Khan et al.[53] also reported in 2002 that the controlled combustion of Ti metal in a natural gas flame could produce carbon-doped $TiO_2$ that can absorb visible light photoelectrochemically to split water with a high efficiency of 8.35% under Xe lamp illumination. However, this photocatalysis performance has been questioned by a number of researchers.[54] A number of reviews[55] have also warned that some of the high efficiency values reported in the literature make use of the current values obtained under potentiostat bias conditions. This makes it difficult to accurately estimate the additional power extracted from the potentiostat to maintain the electrode at a set potential. Several different expressions and methodologies have therefore been used by research groups to find the efficiency, making a direct comparison of reported efficiency values meaningless and hence sparking much debate in the scientific community. The same author has also investigated carbon modified n-type titanium oxide thin films that have shown to give a maximum photoconversion efficiency of 12.9% (under light intensity of 100 mW m$^{-2}$ from a xenon lamp) and photocurrent densities for water splitting of 12.27 mA cm$^{-2}$.[56]

Together with the photocatalysts, some researchers have used cocatalysts (noble metals like Pt and Rh) in order to obtain high activity and reasonable reaction rates. The solid solution of GaN and ZnO modified with nanoparticles of a mixed oxide of rhodium and chromium catalyst[57] gave a 2.5% overall quantum efficiency for overall water splitting at 420–440 nm, an order of magnitude higher than catalysis under visible light. It is noted that the solution was irradiated using a 300 W xenon lamp attached with a cutoff filter. Core (Rh)/shell ($Cr_2O_3$)-structured nanoparticles have been designed as cocatalysts for the GaN:ZnO photocatalyst.[58] A stoichiometric evolution of $H_2$ and $O_2$ was obtained from pure water (Figure 7). With only the $Cr_2O_3$ NPs impregnation of the GaN:ZnO, there is no promotion of the water splitting reaction. On the other hand, using Rh NPs only, there is evolution of $H_2$, but because of the presence of the formed $O_2$, water is formed immediately on the Rh NPs. In the core–shell structure, the Rh core induces the migration of photogenerated electrons from the GaN:ZnO bulk, and the $Cr_2O_3$ shell provides a hydrogen evolution site while preventing water formation on Rh. Nanostructures like nanotubes, nanowires, and nanorods are also used in PEC water splitting because they are expected to exhibit better transport properties than nanoparticles. Nanostructured rod-like morphology of hemeatite ($\alpha$-$Fe_2O_3$) gave a photon-to-current efficiency of about 8% (using 300 UV lamp and a computer controlled 1/8 m monochromator assisted by an automatic filter wheel with a light intensity of 1 mW cm$^{-2}$ at 470 nm), indicating that nanorods improve the transportation of carriers and reduce the recombination losses at grain boundaries.[59]

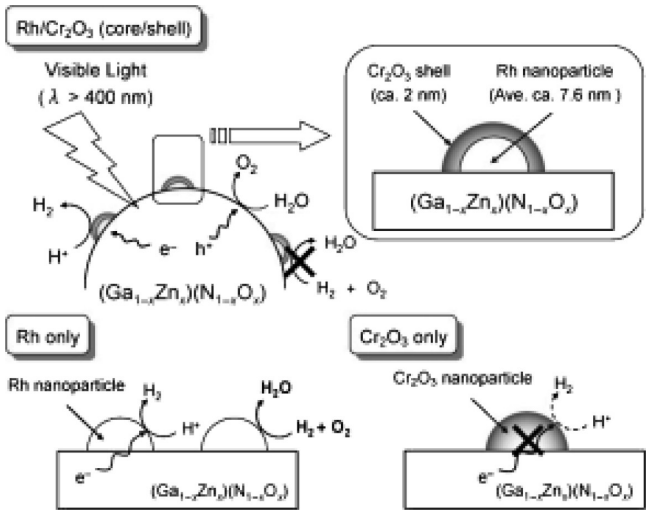


**Figure 7.** Schematic reaction mechanism of water splitting on a core/shell nanococatalyst (reproduced with permission from John Wiley and Sons).[58a]

A number of other studies have been performed on nanorod arrays using $TiO_2$,[60] ZnO,[61] and $KNbO_3$[62] as semiconductors to demonstrate the unique advantages of these structures. More recently, it was observed that by using well-dispersed ($Cd_{0.8}Zn_{0.2}$) single crystal nanorods, efficient and stable photocatalytic $H_2$ evolution could be obtained from water splitting. The nanorods exhibited wide visible light absorption up to 550 nm, and the photocurrent of the anode was three times higher than that of the pure CdS.[63] When using single-crystalline hexagonal prism $Zn_2GeO_4$ nanorods with different aspect ratios, it was observed that there was a boost in the photocatalytic activities in overall water splitting and photoreduction of $CO_2$. This improvement was due to the low crystal defects, high surface area, and beneficial microstructure on the catalyst's surface.[64]

Another effective way to shift the bandgap of the photoelectrodes is by combining the semiconductors with other elements/compounds to form hybrid semiconductor nanomaterials. The other advantage of such a material is the suppression of the recombination of the photogenerated electrons and holes leading to an improvement in the water-splitting reaction efficiency. One approach is to dope the semiconductors with metal ions such as iron or copper or nonmetal species such as silicon and carbon. Mesostructured $CeO_2$ nanoparticles were doped with $La^{3+}$ or $Zr^{4+}$. $CeO_2$ nanoparticles gave a red shift of about 80 nm on the absorption spectrum as compared to $TiO_2$, which leads to a considerably better response in the visible region of the solar spectrum.[65] Another study used a metal plasma ion implantation technique to incorporate trace amounts of transition metal ions of Cu, Ni, V, and Fe into nanoscale anatase $TiO_2$ thin films. This resulted in increased photosensitivity of $TiO_2$ in the visible light regime.[66] A semiconductor photocatalyst $CsTaWO_6$ (3.8 eV) was anion doped with sulfur and sulfur/nitrogen co-doping, resulting in decreased bandgaps (2.06 eV). The doped $CsTaWO_6$ crystals showed a clear improvement in the photocatalytic performance tests and were more efficient in $H_2$ production under simulated solar irradiation, in contrast to the undoped $CsTaWO_6$ or P25. Co-doped $CsTaWO_{6-x-y}S_xN_y$ turned out to be the best material for $H_2$ production because of its capability in efficiently utilizing the visible light in the solar spectrum.[67] Nonmetal doping using nitrogen or carbon on photoelectrodes like $TiO_2$ has also been extensively studied. One pioneering study postulated that the narrowed bandgap of $TiO_2$ contributed to the visible light absorption of nitrogen-doped $TiO_2$ by mixing O 2p states with the N 2p states of the substituted nitrogen atoms.[68] A few years later, other mechanisms were proposed. The isolated N 2p states formed above the valence band were the origin of the visible light absorption band,[69] or the visible light band of nitrogen-doped $TiO_2$ originated from the localized states of the oxygen deficiencies caused by nitrogen doping.[70] The arguments on the origin of the visible light absorption by nitrogen doping have continued, and Serpone[71] suggested that the origin of the absorption is the color centers formed in the bandgap due to the $TiO_2$ reduction after heat treatment. Recently, another research group came up with a sensitization mechanism in which melamine condensation products act as visible light sensitizers.[72]

Sensitization is also another method to increase the photoactivity whereby commonly extra materials (dyes or semiconductor quantum dots) are used to absorb complementary light to that of the primary semiconductor.[73] The semiconductors serve as substrates with high surface areas to which the dye molecules are attached, and higher dye concentration yields optically active photoanodes (semiconductors) that absorb much visible light. For instance, nanoparticulate anatase $TiO_2$ was sensitized with ruthenium polypyridyl dyes which not only served as a sensitizer for visible light absorption but also as a stabilizer to connect water oxidation catalyst $IrO_2 \cdot nH_2O$ NPs. In the solar cell (Figure 8),

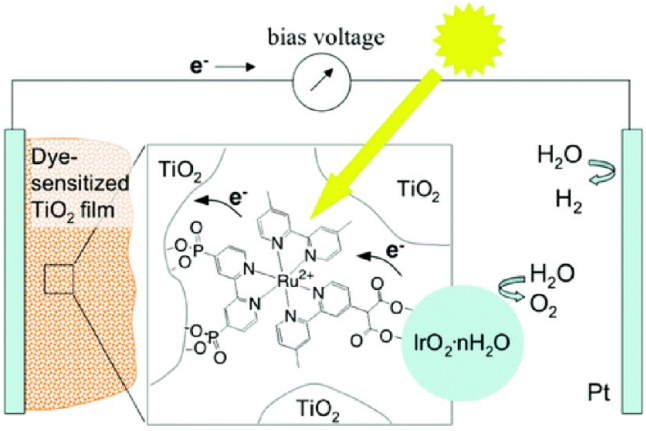


**Figure 8.** Schematic of the water splitting dye sensitized solar cell (reproduced with permission from the American Chemical Society).[74]

upon pulsed laser excitation, electrons are transferred from the excited state of the dye molecules to the $TiO_2$ NPs followed by transfer from the $IrO_2$ NPs to the photo-oxidized dyes. The holes on the $IrO_2$ surface oxidize water, while the electrons transfer to the cathode for hydrogen generation. In place of photosensitive dyes, semiconductor QDs can be used to increase the absorbance of the photoanode for visible light. The absorption spectrum of QDs can be matched with the solar spectrum by altering particle size to generate multiple electron−hole pairs per photon.

Recently,[75] QDs deposited on ZnO nanowires surfaces showed a photocurrent density of three times that of pristine ZnO nanowires of similar thickness, with a maximum photoconversion efficiency of 1.8%. The water-splitting photo-

electrode was illuminated under a xenon lamp that was equipped with filters to simulate the AM1.5 spectrum (390–770 nm, which is in the visible region).

A recently emerging field is the use of plasmonic materials like plasmonic lasers, surface plasmon-enhanced light-emitting diodes, metamaterials, plasmon focusing devices, and plasmon waveguides. Plasmon enhancement can be used for semiconductors having inadequate light absorption. They can either capture the light that would otherwise pass through the thin film if the particles were not there or absorb the photons and then transfer the energy to the adjacent semiconductor.[76] One study found that gold nanoparticles supported on P25 titania ($Au/TiO_2$) exhibit photocatalytic activity for UV and visible light (532 nm laser or polychromatic light $\lambda > 400$ nm) for water splitting. When absorbing irradiation, the gold NPs can inject electrons into the conduction band of the semiconductor, and the localized surface plasmon resonance may be able to induce an electromagnetic field close to the metal materials' surface, hence, enhancing the solar energy conversion efficiency of water splitting. Gold loading, particle size, and calcination temperature influence the photocatalytic activity with a typical 7.5% quantum $H_2$ yield and 5% $O_2$ yield at 560 nm. The most active catalyst contained 0.2 wt % gold with an average particle size of 2 nm. Here, the suspensions were irradiated for 3 h using either a 200 W xenon-doped mercury lamp or the second harmonic of a Nd:YAG laser.[77] Similarly, plasmonic enhancement was demonstrated for $TiO_2$, where a 66-fold enhancement was observed using gold NPs (Figure 9).[78]

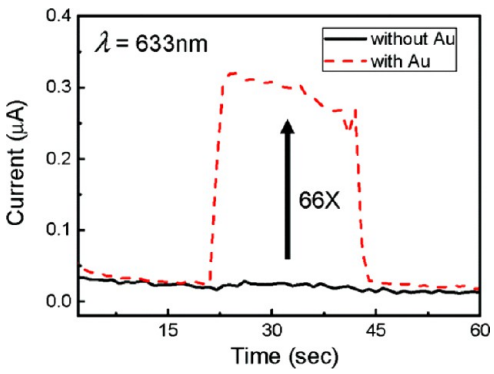


**Figure 9.** Photocurrent of anodic $TiO_2$ with and without Au nanoparticles under $\lambda = 633$ nm light irradiation for 22 s (reproduced with permission from the American Chemical Society).[78]

It was inferred that the plasmonic NPs could effectively couple with visible light from the far-field to the near-field at the surface of the semiconductor. Hence, the region close to the interface between the semiconductor and the plasmonic nanostructure can absorb light to increase the generation of photoinduced carriers. For $\alpha$-$Fe_2O_3$ photoanodes with gold NPs, the enhancement was only observed for electrode geometries with metal particles that were localized at the semiconductor–electrolyte interface.[76]

## ■ BIOFUELS

Increased demand in transportation fuels, environmental concerns, and depletion of fossil fuel require development of efficient conversion technologies for second-generation biofuels.[79] Furthermore, the Federal Renewable Fuels Standard requires the blending of 36 billion gallons of renewable fuels into transportation fuels by 2022.[80] As of now, only a very small fraction of the demand is met by renewable fuels.[81] Currently, the demand for renewable fuels is covered by the production of starch-derived ethanol and oil seed-derived biodiesel. Biomass is regarded as one of the most viable options because it is the largest primary resource, and it is clean and has zero net emissions of carbon dioxide.[82] Biomass to biofuel conversion by thermochemical routes can be achieved via direct liquefaction to fuels or by gasification to synthesis gas followed by conversion to diesel via the Fischer–Tropsch process.[83] Biomass typically contains 20–30 wt % hemicelluloses, 40–50 wt % cellulose, and 20–30 wt % lignin,[84] along with a number of inorganic compounds in small amounts. These constituent biopolymers are composed of long-chain oxygen-rich molecules, and they require different catalysts than the petroleum industry. To this effect, the use of catalysts is needed to facilitate the chemistry by which cellulose- and lignin-derived molecules can be converted to fuels.[1] Most pathways involve the conversion of biomass to syngas or biofuels and the upgrading of the unstable flash pyrolysis or liquefaction products by the use of selective nanocatalysts for reactions like aqueous-phase processing to produce selectively targeted alkanes from glucose, aldol condensations requiring base catalysts, hydrogenation reactions needing metal catalysts, and bifunctional dehydration/hydrogenation reactions with metal/acid catalysts. In this section, selective processes where NPs have been used for the conversion of biomass to biofuels is presented.

## ■ TRANSESTERIFICATION TO PRODUCE BIODIESEL

Biodiesel (an alternative to fossil diesel) is produced via transesterification of oils as per the following reaction:

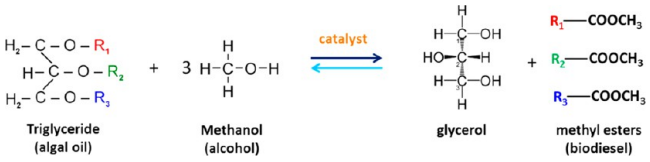


Biodiesel is biodegradable, nontoxic, and can be obtained from various renewable sources, among which are algae. Algal biofuels face a number of challenges such as the difficulty to achieve consistent industrial-scale algae production, high production, and harvesting costs and energy-intensive lipid extraction processes.[85] The conversion of algae to biofuel can be achieved mainly through anaerobic digestion, supercritical fluid treatment, pyrolysis, and gasification. The enzyme-based technologies suffer from low catalytic efficiencies of enzymes, high cost, poor catalysts recovery, and a need for high temperatures and strong acids to transform the feedstock produced.[86] Nanoscale materials provide increased surface area for enzyme loading and help to increase the diffusion rate of substrates to the enzymes, thereby increasing production rates.[87] For example, lipase enzyme from *Candida rugosa* were successfully immobilized in polyvinyl alcohol nanofibrous membranes. Enzyme loading in these bicomponent fibers reached as high as 50%. The lipase-loaded bicomponent fibers exhibited far superior activity than the crude enzyme following exposures to elevated temperatures and humidity. They also possessed far superior stability, i.e., 100, 8, and 3 times longer half-lives than crude lipase following storages at 40 bar, 21 °C, and 65% relative humidity and ambient condition.[88] Recently, a nanofarming technology has been developed that uses nanoparticles to extract oil from algae without harming the

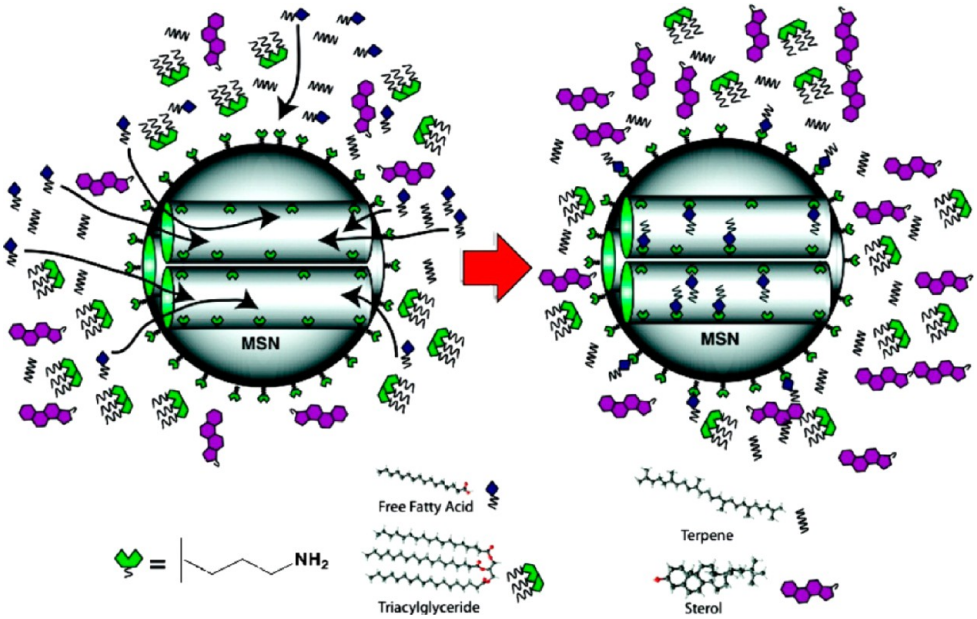


**Figure 10.** Selective uptake and sequestration of free fatty acids from a solution of lipids and hydrocarbons found in algal oil (reproduced with permission from the American Chemical Society).[90]

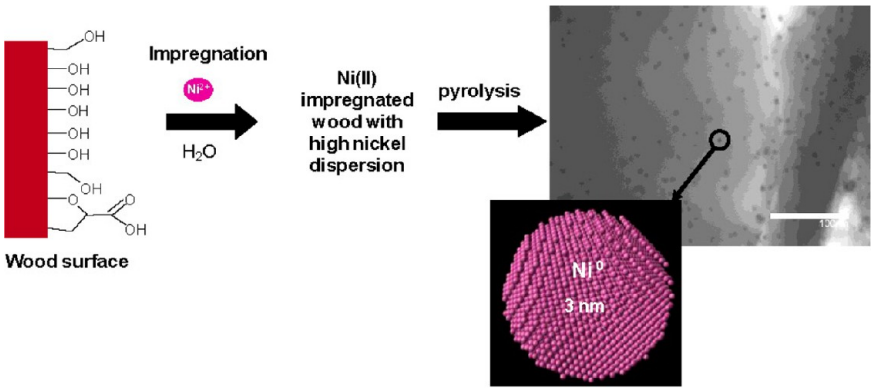


**Figure 11.** Ni(II) impregnated wood before pyrolysis (reproduced with permission from Elsevier Science).[100]

algae (Figure 10). The extracted oil is then converted to biodiesel by transesterification.[89] Here, amine functionalized 10 nm mesoporous silica nanoparticles are used for the selective sequestration of free fatty acids from algae.[90]

For conversion of oil into diesel, several advancements have been made utilizing nanocatalysts. Nanosized calcium oxide with crystallite size of 20 nm gave 99% conversion of soybean oil to biodiesel, while commercial CaO NPs of size 43 nm yielded only 2% biodiesel. The soybean oil/methanol ratio was 1:27, and deactivation was observed after eight cycles. SEM analysis revealed that the fresh catalyst consists of numerous crystallites with well-defined edges, while the same catalyst after seven cycles had formed aggregated polycrystallites with substantially less well-defined edges, hence explaining the deactivation.[91] In another study, cesium was incorporated in nanocrystalline MgO through coprecipitation under supercritical conditions to generate $Cs_2Mg(CO_3)_2$ nanocrystallites with an enhanced density and strength of the surface base sites. This strong synergy between the two components enhanced the rate of tributyrin transesterification with methanol compared to the results obtained with undoped MgO and homogeneous $Cs_2CO_3$ catalysts. The nanocatalyst however suffers from poor recyclability due to heavy surface carbon deposition.[92]

In one study, solid base hydrotalcite-derived nanoparticles with Mg/Al molar ratio of 3/1 were used for the transesterification of *Jatropha* oil in an ultrasonic reactor to obtain a biodiesel yield of 95%. Because of the surface absorption of the glycerol byproduct as well as the collapse of the layered structure, the catalyst underwent deactivation.[93] Calcium aluminate-loaded $Fe_3O_4$ nanoparticles gave a biodiesel yield of 99%. Also, the activity and recovery rate of this catalyst was maintained after 5 cycles of catalysis because having magnetic properties made the catalyst easy to separate.[94]

## ■ BIOMASS GASIFICATION AND PYROLYSIS

Nanomaterials can provide particularly high surface area to mass ratio, which is desirable for catalysis and control of chemical composition. In fact, specific matching of catalysts with reactor types and processes is one of the other benefits of using nanoscale.[95] Gasification converts carbon-containing feedstock into a synthetic gas comprising of hydrogen, carbon monoxide, etc.[96] Gasification of biomass into fuel gases, such as synthesis gas or producer gas, is a promising route to produce

renewable fuels, which is commonly accomplished via partial oxidation of the feedstock using substoichiometric air or oxygen or by indirect heating with or without steam. Hao et al.[97] gasified cellulose and sawdust in supercritical water to produce a gas rich in hydrogen and investigated the use of a suite of nanocatalysts including $CeO_2$ and $(CeZr)_xO_2$. Increased $H_2$ production coincided with an increase in the catalyst's surface area per mass. Another study investigated methane decomposition reactions to form hydrogen and nanocarbon on a nickel-based nanocatalyst. The catalysts have been designed to stabilize nanoscale metal particles that act as a growth tip for the nanocarbons. It was found that temperatures higher than 800 °C render the process more commercially viable due to the amount of hydrogen production. A one-pot synthesis method allowed a metal precursor (nickel acetylacetonate) to reduce directly onto the surface of the carbon nanotube/fiber without the pretreatment of surface functional groups to form carbon nanotube/fiber and aluminosilicate-supported Ni catalysts. The catalysts were used for biomass gasification in supercritical water for the production of hydrogen-rich gases. Compared to the two commercially available aluminosilicate-supported Ni catalysts, the synthesized catalysts produced similar hydrogen yields (~8 mmol $H_2$/g biomass), but the $H_2/CH_4$ mole ratio for the synthesized catalysts was 3.5 compared to 1.3 for the commercial catalysts.[98]

Pyrolysis, thermal decomposition of materials in the absence of oxygen, is another method to upgrade bioderived feedstocks to fuels.[99] The strategy of impregnating lignocellulosic biomass with aqueous metal salts solutions was investigated for producing $H_2$-rich gas by pyrolysis of wood (Figure 11). During the pyrolysis, formation of nickel metal NPs was studied. It was postulated that during the wood impregnation step, the oxygenated groups present in the biomass act as adsorption sites for metal cations in the aqueous medium. This leads to very high metal precursor dispersion into the wood matrix. Subsequently, during pyrolysis, an amorphous $Ni_xO_yH_z$ phase is formed. This phase is then reduced to metallic nickel ($Ni^0$) by carbon atoms at temperatures below 500 °C, leading to the formation of $Ni^0$ NPs. The so formed $Ni^0$ nanocrystallites act as the catalytic active phase for enhancing both $H_2$ production and tar conversion during the initial stage of biomass pyrolysis.[100]

During biomass gasification/pyrolysis, along with the generation of useful products (fuel gases, char), many byproducts such as fly ash, $NO_x$, $SO_2$, and tar are also formed. Tar is a complex mixture of condensable hydrocarbons, which includes single-ring to 5-ring aromatic compounds along with other oxygen-containing hydrocarbons and complex PAHs.[101] This so-formed tar will be condensed as temperature is lower than its dew point, and then block and foul process equipment like fuel lines, filters, engines, and turbines. The tar content in the syngas from an air-blown circulating fluidized bed biomass gasifier was reported to be about 10 g/m$^3$. Most applications of product gases require a low tar content, on the order 0.05 g/m$^3$ or less.[102] Hence, tar disposal becomes one of the most necessary and urgent problems during biomass gasification. A novel $Al_2O_3$-supported nano-NiO catalyst for tar removal in biomass gasification/pyrolysis was developed so as to significantly enhance the quality of the produced gases.[103] The supported nano-NiO/$\gamma$−$Al_2O_3$ catalyst was prepared by a deposition−precipitation (DP) method. Various analytical methods revealed that the nano-NiO/$\gamma$−$Al_2O_3$ catalysts had a coated structure with a 12 wt % loading of NiO resulting in a higher surface area when compared to commercial nickel-based catalysts. The active spherical NiO nanoparticles had a size range of 12−18 nm. During biomass pyrolysis, the tar removal efficiency reached up to 99% for catalytic pyrolysis at 800 °C with a marked increase in the gas yield. The $CO_2$ and $CH_4$ percentages in the product gas after addition of the catalysts were reduced, while those of the valuable $H_2$ and CO strongly increased. This gas yield increase was attributed to be predominantly through secondary cracking of the pyrolysis vapors (which would otherwise form tar) on the catalyst in the catalytic bed reactor. The NiO/$\gamma$−$Al_2O_3$ catalyst enhanced the cracking of tar in vapor and of hydrocarbons such as $CH_4$ and $C_nH_m$ to $H_2$ and CO. The same research group[104] also looked into the use of nano-NiO particles as catalysts in biomass pyrolysis. These spherical nano-NiO particles (mean size of ~7.5 nm and specific surface area of 188.0 m$^2$/g) were prepared via precursors, which were obtained by homogeneous precipitation involving an aqueous solution of nickel nitrate hexahydrate and urea. Pyrolysis of the three biomass components, namely, cellulose, xylan, and lignin, were investigated. Compared to a commercial Ni-based catalyst, the weight loss of the biomass components occurred at relatively lower temperatures with low residues. It was postulated that the catalyst promoted the devolatilization and thermal degradation of biomass. This could be due to the possible formation of weak bonds between volatiles and the catalyst, causing other bonds in the volatile molecule to be stretched and weakened. The authors postulated that a possible new reaction pathway decreased the activation energy of biomass-derived components. The nanocatalyst (in particular, particles with a size of ~7.5 nm) also accelerated primary and secondary decomposition reactions of biomass that could then occur at a lower temperature.

## HYDROGENATION OF BIOMASS-DERIVED COMPOUNDS

Biomass-derived compounds need to be hydrogenated or hydro-deoxygenated in order to produce useful fuels and chemicals, and several nanocatalysts have been tested to enhance these reactions. For example, 5-hydromethylfurfural (HMF) has been successfully synthesized from fructose, glucose, and cellulose using different catalysts, including nanocatalysts.[105] HMF can be converted to 2,5-dimethylfuran (DMF) via hydrogenation or to levulinic acid (LA) via an acid-catalyzed ring-opening process.[106] LA is a biomass-derived platform molecule and serves as precursor for liquid fuels like $\gamma$-valerolactone (gVL).[107] Highly dispersed metal nanoparticulates on metal oxide supports have shown to be efficient for aerobic oxidation of HMF with gold showing marked chemoselectivity. One study[108] reported the remarkable development of an HMF oxidation/esterification process using Au on a $TiO_2$ support. The reactions were run at 130 °C and 4 bar $O_2$ in methanol with MeONa as base. A high yield of 98% 2,5-furandimethylcarboxylate (FDMC) was obtained. The authors proposed an oxidation pathway of HMF to FDMC via the hemiacetal intermediates. Another investigation[109] was performed using Au on $CeO_2$ to catalyze biomass-derived HMF oxidation into FDCA but without a base. The results revealed that the catalytic performance of Au/$CeO_2$ depends on the particle size of the catalyst. Decreasing the particle size led to an increase in external-to-internal atom ratio resulting in high populations of unsaturations. Unsaturations, as described in the study, are defect sites, mainly oxygen vacancies, formed in the

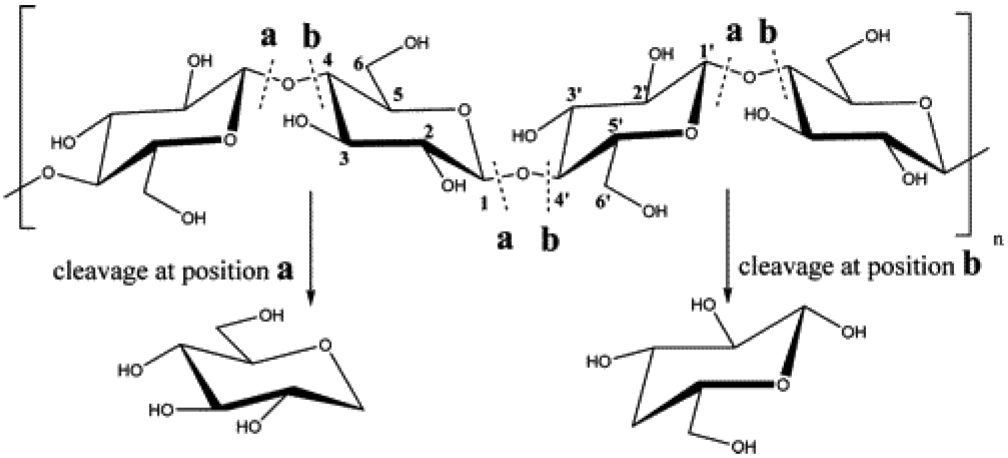


**Figure 12.** Cellulose structure and potential monomers formed following cleavage of the C−O−C bonds at position a or b (reproduced with permission from the American Chemical Society).[116]

presence of $Ce^{3+}$. The increase in the population of defects resulted in enhanced adsorption and redox potential of the catalysts. A number of studies have investigated the use of gold for the oxidation of HMF including using $TiO_2$- and carbon-supported Pt, Pd, and Au[110] catalysts, hydrotalcite-supported Au NPs,[111] and gold−copper bimetallic nanoparticles[112] over $TiO_2$.

Two reactions, namely, the aqueous oxidation of benzyl alcohol and the hydrogenation of furfural in water were tested under microwave irradiation using carbon-supported Pd nanoparticles. The most active nanocatalysts were trioctylphosphine- and triphenylphosphine-stabilized Pd NPs on oxidized carbon support. The presence of oxygen groups on the surface of the carbon support, particularly those of acidic character, improved the Pd NPs immobilization as well as the water affinity and, consequently, the catalytic performances of the system.[113] One group[114] examined the vapor-phase furfural decarbonylation/hydrogenation reaction network as a function of Pt nanoparticles with various particle sizes (1.5−7.1 nm size range) and shapes (rounded, cubes, octahedral). The Pd NPs were encapsulated in poly(vinylpyrrolidone) (PVP) and dispersed on MCF-17 mesoporous silica. The reaction conditions were ambient pressure in the 443−513 K range. Furfural decarbonylation and hydrogenation reactions yielded mainly furan and furfuryl alcohol (FFA), respectively. In both reactions, the structure of the catalysts brought about changes in product selectivities, turnover rates (TORs), and apparent activation energies ($E_A$ values). Small particles were found to give predominantly furan as a product, via decarbonylation, while larger-sized particles yielded both furan and furfuryl alcohol. Octahedral particles were observed to be selective to furfuryl alcohol, while cube-shaped particles produced an equal amount of furan and furfuryl alcohol. The differences in selectivity have been attributed to the presence of two different catalytically active sites that change in ratio with NP size and shape.

Hydrogenation of succinic acid (SA) in aqueous ethanol under mild reaction conditions was investigated using a variety of highly active, stable, and reusable supported metal nanoparticles (SMNPs) including Pt, Pd, Rh, and Ru (5% loading) on a mesoporous material derived from biomass (Starbon−SMNPs).[115] The versatility of the functional groups as well as its stability under aqueous conditions makes Starbon-300 a good candidate. Ru−Starbon and Pt−Starbon catalysts exhibited the highest conversion because they were smaller and evenly dispersed. The selectivity was also significantly different for Ru−Starbon; 60−82% tetrahydrofuran (THF) was obtained, while Pd, Pt, and Rh−Starbon materials were more selective to 1,4-butanediol (BDO). The reaction conditions could also be tuned to maximize $\gamma$-butyrolactone (GBL) production from Pd−Starbon or Ru−Starbon (up to 65% selectivity at 45% conversion—10 h reaction—using 5% Pd−Starbon). Interestingly, the catalysts were found to preserve over 95% of their initial activity even after five reaction cycles. One-step conversion of cellobiose to C6-alcohols was achieved by selectively breaking the C−O−C (glycosidic) bonds (Figure 12) via hydrogenation using water-soluble transition metals (Ru, Rh, Pd, or Pt) nanocluster catalysts under $H_2$ pressure in ionic liquid. Ru was the only metal that exhibited high stability under the reaction conditions (120 °C and 40 bar of $H_2$) and gave high activity and selectivity, that is, the cellobiose was quantitatively converted to C6-alcohols. This concept creates new opportunity to transform cellulose into biofuels and other useful value-added chemicals.[116]

A continuous process was designed in which two homogeneous phases coexisted with an emulsion in a layered configuration of oil/emulsion/water.[117] Bearing in mind that carbon nanotubes, being hydrophobic, have been shown to produce emulsions, hybrid nanoparticles were prepared by fusing carbon nanotubes to silica. By tuning their composition, the hydrophilic−hydrophobic balance could be modified. These nanohybrids were studied by incorporating a transition metal, rendering them catalytically active for hydrogenation. The Pd particles still sit in the organic/aqueous interface, and the emulsions formed are unaffected. Depositing a metal such as Pd on the hydrophilic face would catalyze aqueous reactions, whereas deposition on the hydrophobic face would favor chemistry in the organic solvent. Full conversion can therefore be achieved on both sides of the emulsion by constant removal of products formed from both the top and bottom layers because the reaction occurs in the emulsion phase.

One of the ways to upgrade biomass-derived bio-oil is by hydrodeoxygenation (HDO) through the use of catalysts to remove oxygen (from the oxygenated compounds found in bio-oil) as CO, $CO_2$, or $H_2O$. In one study,[118] a task-specific ionic liquid (3-methyl-1-butylpyridine dicyanamide) was used as a precursor with silica NPs as a hard template to yield a high nitrogen content (12 wt %) mesoporous carbon material. This

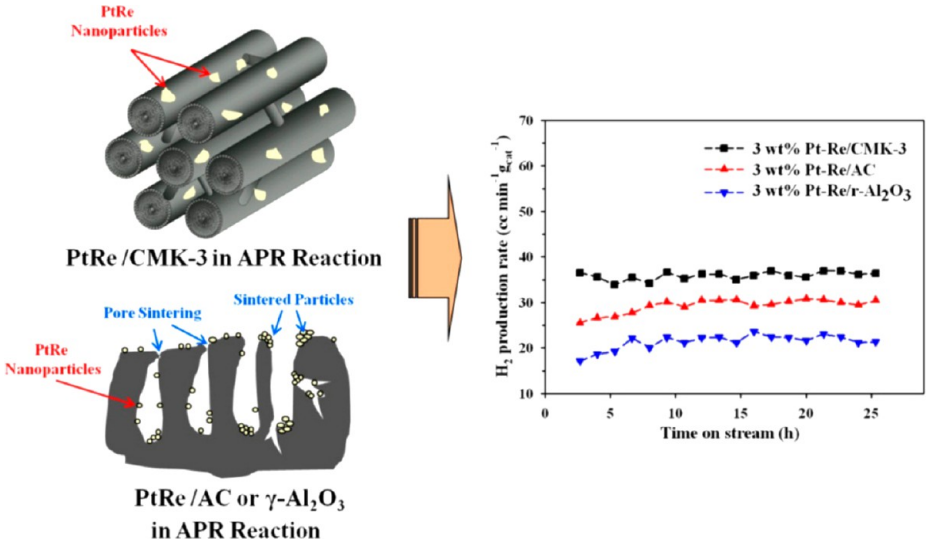


**Figure 13.** Hydrogen production rates when using PtRe NPs on different supports (reproduced with permission of Elsevier BV).[122]

material could stabilize Pd NPs, and the resulting Pd@$CN_{0.132}$ (Pd nanoparticles supported on mesoporous N-doped carbon) catalyst exhibited a high activity for the hydrodeoxygenation of vanillin, a common component in lignin-derived bio-oil. The reaction conditions were mild with low hydrogen pressure and water as a clean solvent. A 100% conversion of vanillin and 100% selectivity for 2-methoxy-4-methylphenol were achieved, and the catalyst did not lose its activity after six recycles. The special structure of the catalytic N-doped carbon−metal heterojunction led to a very stable and uniform dispersion of Pd NPs and promoted additional electronic activation of the metal NPs as well as a good dispersion of the catalyst in water. The high catalytic performance of Pd@$CN_{0.132}$ reveals a promising potential for the biofuel upgrade process. Simultaneous condensation and hydrogenation of biomass-derived oxygenates in water/oil emulsions stabilized by amphiplilic nanohybrid catalysts were also investigated.[119] The emulsion system leads to an enhancement in the mass transfer between phases due to a larger interfacial area. For instance, it was found that the aldol-condensation reaction of furfural and acetone is more effective in an emulsion system than in a single aqueous phase. In addition, the presence of the two phases facilitated the separation of the products. Among the different basic oxides employed to grow carbon nanotubes (CNT) on their surface, the nanohybrids supported on MgO have shown to be the most effective for aldol condensation. Active metals such as Pd or Pt were incorporated onto the nanohybrids to facilitate the hydrogenation of the aldol condensation products in the same emulsion system. Increasing the temperature led to the formation of fully deoxygenated long-chain alkanes (tridecane).

## ■ REFORMING OF BIOMASS-DERIVED COMPONENTS

Aqueous-phase reforming (APR) can produce hydrogen and carbon monoxide (synthesis gas) from biomass-derived molecules at mild temperatures of 220−320 °C in liquid phase by utilizing a suitable nanocatalyst (e.g., Pt, Ru, and Pt−Ru).[1] This one-pot reaction process can produce hydrogen and reduced sugars simultaneously.[120] For example, APR was utilized to convert glycerol into 1,2-propanediol (1,2-PDO) using 5 wt % Ru/$Al_2O_3$ mixed with 5 wt % Pt/$Al_2O_3$ catalyst, without any added hydrogen. A glycerol conversion of 50.1% and a 1,2-PDO selectivity of 47.2% were obtained. When the same reaction was carried out with added hydrogen (41 bar), a lower selectivity to 1,2-PDO (31.9%) was obtained because the excess hydrogen promoted the transformation of CO and $CO_2$ to methane and other alkanes, adversely affecting the 1,2-PDO selectivity.[121] Aqueous phase reforming of polyol over the supported Pt−Re bimetallic catalyst has been attempted, and the activity of supported 3 wt % Pt−Re catalysts was found to be as follows: $Al_2O_3$ < $SiO_2$ < activated carbon < CMK-3(ordered mesoporous carbon). The reason why a CMK-3-supported catalyst exhibited the highest catalytic activity for APR reaction (Figure 13) is due to easy accessibility to its metal catalytic active sites, easy escape of product gas, and a high metal dispersion. It was observed that the conversion of carbon to gas and hydrogen yield increased with both temperature and corresponding system pressure. Low weight hourly space velocity also favored hydrogen yield and conversion of carbon to gas without decreasing the selectivity of hydrogen and alkane.[122]

The effect of support properties on catalytic performance for APR of 5 wt % glycerol was studied by loading MgO, $Al_2O_3$, $CeO_2$, $TiO_2$, and $SiO_2$ catalysts on presynthesized Pt colloids on the supports. By measuring the conversion of glycerol, rate of hydrogen production, and composition of gaseous products, it was found that the overall catalytic activities decreased in the following order: Pt/MgO > Pt/$Al_2O_3$ > Pt/$CeO_2$ > Pt/$TiO_2$ > Pt/$SiO_2$. WGS played a key role in the process of APR because both are related to the surface properties. It was postulated that WGS preferred the basic sites and further enhanced the APR.[123]

A carbon-supported PtMo catalyst was used for the aqueous phase reforming of glycerol to produce hydrogen. Using X-ray absorption spectroscopy (XAS), it was found that the catalyst consisted of bimetallic nanoparticles with a Pt-rich core and a Mo-rich surface with approximately 25% of the surface atoms being Pt. The fresh PtMo NPs were about 2 nm, and after 30 days of glycerol reforming at 31 bar and 230 °C, they increased in size to about 5 nm.[124] Other types of supported (CMK-3, commercial activated carbon (AC), and alumina) Pt-based bimetallic catalysts (Pt−Re, Pt−Mn, Pt−Fe, Pt−Cs, Pt−Ba, Pt−Ga, Pt−Ag, and Pt−Mo) were tested for hydrogen production via APR of ethylene glycol. The 1:1 Pt:Mn molar

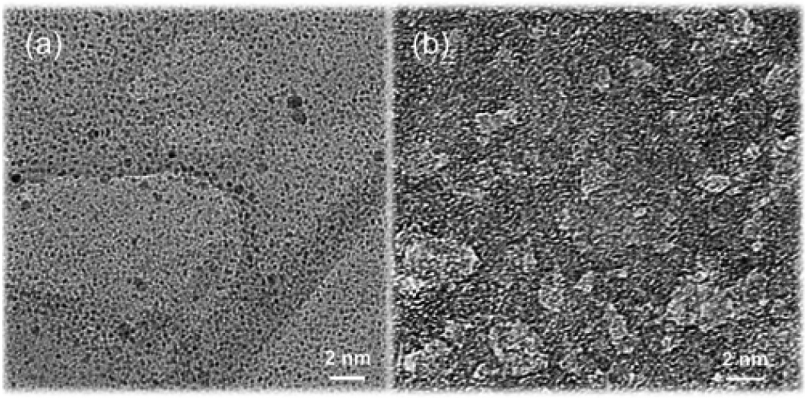


**Figure 14.** TEM images of (a) spent Cu/reduced graphene oxide (rGO) (after first run) and (b) CuPd/rGO (after third recycle) catalysts (reproduced with permission from the American Chemical Society).[126]

ratio significantly enhanced the catalytic performances because of the interaction between the Pt and Mn species to form Pt−Mn alloys supported on CMK-3. Out of all the supports, the CMK-3 support demonstrated better performance than the commercial AC and alumina. Therefore, it was concluded that the catalytic performance of the APR reaction over Pt−Mn/CMK-3 catalyst depended on the alloy effect as well as the structural properties and nature of the support.[125] Recently, a new family of surface facet-controlled bimetallic Cu-based nanocatalysts supported on the graphene derivative has been synthesized.[126] Their unique surface configuration show exceptional activity and stability for aqueous phase biomass conversion. Using the graphene derivative as a 2-D template, the directed growth of dominant reactive surface facets of Cu nanocrystals (Cu{111})[102,119] was achieved by lattice-match engineering. These Cu-graphene catalysts were used for converting biopolyols (glycerol, xylitol, and sorbitol) to value-added chemicals, such as lactic acid and other useful coproducts consisting of diols and linear alcohols. Furthermore, trace amounts of Pd was incorporated to enhance activity and stability so that the hydrogen generated in situ from polyols is used for sequential hydrogenolysis of the feedstock. Figure 14 illustrates how the addition of Pd enhances the stability whereby no significant leaching is found on the spent catalyst (Figure 14b), whereas Cu has obviously leached in the Cu/rGO catalyst in Figure 14a.

Steam reforming of biomass-derived oxygenates like ethanol yield hydrogen that can be used as an energy source for fuel cell applications. Steam-reforming catalysts need to be active, stable, and display high selectivity for $H_2$. One study[127] synthesized Co nanoparticles (∼5 nm) on an inert support (graphitized-activated carbon, g-AC). Acetone was used as a model compound because it is the intermediate observed in ethanol and acetic acid steam reforming, has characteristic bonds found in biomass-derived oxygenates, and is a key component in butanol derived from fermentation. DFT calculations revealed that the Co nanoparticles served to cleave the C−C bond of acetone, while efficiently dissociating $H_2O$ to oxidize $CH_x$* and C*. The high selectivity of the supported Co NPs to $H_2$ is attributed to facile scission of the C−H bond relative to that of the C−C bond of acetone. The exceptional stability of the catalyst is due to enhanced oxygen mobility by facile water dissociation on the Co nanoparticles and the lack of acid/base sites on the inert support. Therefore, acetone (either as a byproduct or as a reactant) can be selectively steam reformed to produce hydrogen without any catalyst deactivation issues. Fundamental understanding of the nature of nanoparticles is needed to provide further insight into the rational design of catalysts for upgrading of bio-oil.

## ■ SUMMARY

Even though nanotechnology as a new area of technology still faces many challenges like reliability, safety, lifetime, and costs, it has also demonstrated promising results in the field of sustainable energy applications, as pointed out by many examples in this review. During the last two decades, the design of photoactive nanostructure architectures and inorganic−organic hybrid systems has made significant progress. Quantum dot- and carbon nanostructure-based solar cells are still in their early developmental stage but provide opportunities for the development of the next generation of PV.[12]

For water-splitting photoelectrochemical cells, the efficiency is still very low, and the development of high-efficiency and cost-effective materials would render this technology more economically viable. For this particular technology, it is suggested to gear future research toward the development of (i) sensitization materials with multi-absorption regions in visible light, (ii) infrared active materials to harvest a great part of the solar spectrum, and (iii) defect-free photoactive materials for the visible region (improved architectures and properties). Furthermore, an increase in the absorption coefficient of photoactive materials and in the yield of photogenerated electron−hole pairs coupled with an improvement of the generation and separation of electron−holes by assisting with additional materials would shift the development of PEC at a commercial scale.[73] In addition, a cost-effective technology to simultaneously separate hydrogen and oxygen would be needed.[128] As for organic solar cells, advanced materials such as thermocleavable polymers for higher level processing and stability in combination with advanced device concepts like tandem cells and ITO free roll-to-roll coating are needed in order to go beyond the current state-of-the art technology.[129] The expectation is that more progress will be made via novel optimized materials as well as more efficient device geometries.

The valorization of biomass is still very much an ongoing area of research due to the fact that it has the tremendous potential of being a source of fuel and value-added chemicals. The use of nanocatalysts can help in maximizing yields, minimizing residues, decreasing environmental impacts, and obtaining products at low costs. The main challenge remains

the complexity of the structure of lignocellulosic biomass. In gasification, for instance, the impurities cause tar formation, while in pyrolysis, the bio-oil formed contains a lot of oxygenated compounds. The separation or purification of bio-oil therefore becomes complex. One solution would be to separate the biomass into fractions (hemicellulose, cellulose, and lignin) in order to produce specialty chemicals and fuels at higher conversions and selectivities.[1] With the materials we have today, we are not able to provide the solutions at the efficiency and cost required, but due to ongoing research in nanotechnology around the world, novel materials are being developed using better material science and engineering expertise so that we can contribute to the well-being of present and future generations.[11]

## ■ AUTHOR INFORMATION

### Corresponding Author

*E-mail: gupta@auburn.edu. Phone: (334) 844-2013. Fax: (334) 844-2063.

### Notes

The authors declare no competing financial interest.

## ■ REFERENCES

(1) Alonso, D. M.; Wettstein, S. G.; Dumesic, J. A. Bimetallic catalysts for upgrading of biomass to fuels and chemicals. *Chem. Soc. Rev.* **2012**, *41* (24), 8075−8098.

(2) Moniz, E. J.; Garcia-Martinez, J. *Nanotechnology for the Energy Challenge*; Wiley-VCH: Weinheim, Germany, 2010.

(3) Mao, S. S.; Chen, X. Selected nanotechnologies for renewable energy applications. *Int. J. Energy Res.* **2007**, *31* (6−7), 619−636.

(4) Faunce, T. A. Governing nanotechnology for solar fuels: Towards a jurisprudence of global artificial photosynthesis. *Renewable Energy Law Policy* **2011**, *2*, 163−168.

(5) Gust, D.; Moore, T. A.; Moore, A. L. Solar fuels via artificial photosynthesis. *Acc. Chem. Res.* **2009**, *42* (12), 1890−1898.

(6) Singh, R. S.; Rangari, V. K.; Sanagapalli, S.; Jayaraman, V.; Mahendra, S.; Singh, V. P. Nano-structured CdTe, CdS and $TiO_2$ for thin film solar cell applications. *Sol. Energy Mater. Sol. Cells* **2004**, *82* (1−2), 315−330.

(7) Etgar, L. Semiconductor nanocrystals as light harvesters in solar cells. *Materials* **2013**, *6* (2), 445−459.

(8) Heston, N. IPCE Monochromator User Guide, Newport Oriel. mccl.chem.ufl.edu/sec/manual/User_Manual_MCCL_IPCE.docx (accessed May 24, 2013).

(9) Hersch, P.; Zweibel, K. *Basic Photovoltaic Principles and Methods*; Solar Energy Research Institute: Golden, CO, 1982.

(10) Nozik, A. J. Nanoscience and nanostructures for photovoltaics and solar fuels. *Nano Lett.* **2010**, *10* (8), 2735−2741.

(11) Serrano, E.; Rus, G.; García-Martínez, J. Nanotechnology for sustainable energy. *Renewable Sustainable Energy Rev.* **2009**, *13* (9), 2373−2384.

(12) Kamat, P. V. Quantum dot solar cells. Semiconductor nanocrystals as light harvesters. *J. Phys. Chem. C* **2008**, *112* (48), 18737−18753.

(13) Leschkies, K. S.; Divakar, R.; Basu, J.; Enache-Pommer, E.; Boercker, J. E.; Carter, C. B.; Kortshagen, U. R.; Norris, D. J.; Aydil, E. S. Photosensitization of ZnO nanowires with CdSe quantum dots for photovoltaic devices. *Nano Lett.* **2007**, *7* (6), 1793−1798.

(14) Luque, A.; Martí, A.; Nozik, A. J. Solar cells based on quantum dots: Multiple exciton generation and intermediate bands. *MRS Bull.* **2007**, *32* (03), 236−241.

(15) Wöhrle, D.; Meissner, D. Organic solar cells. *Adv. Mater.* **1991**, *3* (3), 129−138.

(16) (a) Chen, S.; Ingram, R. S.; Hostetler, M. J.; Pietron, J. J.; Murray, R. W.; Schaaff, T. G.; Khoury, J. T.; Alvarez, M. M.; Whetten, R. L. Gold nanoelectrodes of varied size: Transition to molecule-like charging. *Science* **1998**, *280* (5372), 2098−2101. (b) Chen, S.; Murray, R. W. Electrochemical quantized capacitance charging of surface ensembles of gold nanoparticles. *J. Phys. Chem. B* **1999**, *103* (45), 9996−10000.

(17) Subramanian, V.; Wolf, E. E.; Kamat, P. V. Catalysis with $TiO_2$/Gold nanocomposites. Effect of metal particle size on the Fermi level equilibration. *J. Am. Chem. Soc.* **2004**, *126* (15), 4943−4950.

(18) Subramanian, V.; Wolf, E. E.; Kamat, P. V. Green emission to probe photoinduced charging events in ZnO−Au nanoparticles. Charge distribution and Fermi-level equilibration. *J. Phys. Chem. B* **2003**, *107* (30), 7479−7485.

(19) (a) Nakanishi, T.; Ohtani, B.; Uosaki, K. Fabrication and characterization of CdS-nanoparticle mono- and multilayers on a self-assembled monolayer of alkanedithiols on gold. *J. Phys. Chem. B* **1998**, *102* (9), 1571−1577. (b) Torimoto, T.; Tsumura, N.; Nakamura, H.; Kuwabata, S.; Sakata, T.; Mori, H.; Yoneyama, H. Photoelectrochemical properties of size-quantized semiconductor photoelectrodes prepared by two-dimensional cross-linking of monodisperse CdS nanoparticles. *Electrochim. Acta* **2000**, *45* (20), 3269−3276. (c) Hens, Z.; Tallapin, D. V.; Weller, H.; Vanmaekelbergh, D. Breaking and restoring a molecularly bridged metal vertical bar quantum dot junction. *Appl. Phys. Lett.* **2002**, *81* (22), 4245−4247.

(20) Ginger, D. S.; Greenham, N. C. Charge injection and transport in films of CdSe nanocrystals. *J. Appl. Phys.* **2000**, *87* (3), 1361−1368.

(21) Granot, E.; Patolsky, F.; Willner, I. Electrochemical assembly of a CdS semiconductor nanoparticle monolayer on surfaces: Structural properties and photoelectrochemical applications. *J. Phys. Chem. B* **2004**, *108* (19), 5875−5881.

(22) Costi, R.; Saunders, A. E.; Elmalem, E.; Salant, A.; Banin, U. Visible light-induced charge retention and photocatalysis with hybrid CdSe−Au nanodumbbells. *Nano Lett.* **2008**, *8* (2), 637−641.

(23) Debnath, R.; Tang, J.; Barkhouse, D. A.; Wang, X.; Pattantyus-Abraham, A. G.; Brzozowski, L.; Levina, L.; Sargent, E. H. Ambient-processed colloidal quantum dot solar cells via individual pre-encapsulation of nanoparticles. *J. Am. Chem. Soc.* **2010**, *132* (17), 5952−5953.

(24) Pattantyus-Abraham, A. G.; Kramer, I. J.; Barkhouse, A. R.; Wang, X.; Konstantatos, G.; Debnath, R.; Levina, L.; Raabe, I.; Nazeeruddin, M. K.; Grätzel, M.; Sargent, E. H. Depleted-heterojunction colloidal quantum dot solar cells. *ACS Nano* **2010**, *4* (6), 3374−3380.

(25) Semonin, O. E.; Luther, J. M.; Choi, S.; Chen, H.-Y.; Gao, J.; Nozik, A. J.; Beard, M. C. Peak external photocurrent quantum efficiency exceeding 100% via MEG in a quantum dot solar cell. *Science* **2011**, *334* (6062), 1530−1533.

(26) Hoppe, H.; Sariciftci, N. S. Organic solar cells: An overview. *J. Mater. Res.* **2004**, *19* (07), 1924−1945.

(27) Brabec, C. J.; Durrant, J. R. Solution-processed organic solar cells. *MRS Bull.* **2008**, *33* (07), 670−675.

(28) (a) Li, G.; Shrotriya, V.; Huang, J.; Yao, Y.; Moriarty, T.; Emery, K.; Yang, Y. High-efficiency solution processable polymer photovoltaic cells by self-organization of polymer blends. *Nat. Mater.* **2005**, *4* (11), 864−868. (b) Kim, Y.; Cook, S.; Tuladhar, S. M.; Choulis, S. A.; Nelson, J.; Durrant, J. R.; Bradley, D. D. C.; Giles, M.; McCulloch, I.; Ha, C.-S.; Ree, M. A strong regioregularity effect in self-organizing conjugated polymer films and high-efficiency polythiophene:fullerene solar cells. *Nat. Mater.* **2006**, *5* (3), 197−203.

(29) Campoy-Quiles, M.; Ferenczi, T.; Agostinelli, T.; Etchegoin, P. G.; Kim, Y.; Anthopoulos, T. D.; Stavrinou, P. N.; Bradley, D. D. C.; Nelson, J. Morphology evolution via self-organization and lateral and vertical diffusion in polymer:fullerene solar cell blends. *Nat. Mater.* **2008**, *7* (2), 158−164.

(30) Hauch, J. A.; Schilinsky, P.; Choulis, S. A.; Childers, R.; Biele, M.; Brabec, C. J. Flexible organic P3HT:PCBM bulk-heterojunction modules with more than 1 year outdoor lifetime. *Sol. Energy Mater. Sol. Cells* **2008**, *92* (7), 727−731.

(31) Scharber, M. C.; Mühlbacher, D.; Koppe, M.; Denk, P.; Waldauf, C.; Heeger, A. J.; Brabec, C. J. Design rules for donors in

bulk-heterojunction solar cells—Towards 10% energy-conversion efficiency. *Adv. Mater.* **2006**, *18* (6), 789−794.
(32) Zhu, Z.; Waller, D.; Gaudiana, R.; Morana, M.; Mühlbacher, D.; Scharber, M.; Brabec, C. Panchromatic conjugated polymers containing alternating donor/acceptor units for photovoltaic applications. *Macromolecules* **2007**, *40* (6), 1981−1986.
(33) Peet, J.; Kim, J. Y.; Coates, N. E.; Ma, W. L.; Moses, D.; Heeger, A. J.; Bazan, G. C. Efficiency enhancement in low-bandgap polymer solar cells by processing with alkane dithiols. *Nat. Mater.* **2007**, *6* (7), 497−500.
(34) Park, S. H.; Roy, A.; Beaupre, S.; Cho, S.; Coates, N.; Moon, J. S.; Moses, D.; Leclerc, M.; Lee, K.; Heeger, A. J. Bulk heterojunction solar cells with internal quantum efficiency approaching 100%. *Nat Photon* **2009**, *3* (5), 297−302.
(35) Gur, I.; Fromer, N. A.; Geier, M. L.; Alivisatos, A. P. Air-stable all-inorganic nanocrystal solar cells processed from solution. *Science* **2005**, *310* (5747), 462−465.
(36) Robel, I.; Subramanian, V.; Kuno, M.; Kamat, P. V. Quantum dot solar cells. Harvesting light energy with CdSe nanocrystals molecularly linked to mesoscopic $TiO_2$ films. *J. Am. Chem. Soc.* **2006**, *128* (7), 2385−2393.
(37) (a) Rodriguez, I.; Ramiro-Manzano, F.; Atienzar, P.; Martinez, J. M.; Meseguer, F.; Garcia, H.; Corma, A. Solar energy harvesting in photoelectrochemical solar cells. *J. Mater. Chem.* **2007**, *17* (30), 3205−3209. (b) Carbonell, E.; Ramiro-Manzano, F.; Rodriguez, I.; Corma, A.; Meseguer, F.; Garcia, H. Enhancement of $TiO_2$ photocatalytic activity by structuring the photocatalyst film as photonic sponge. *Photochemical & Photobiological Sciences* **2008**, *7* (8), 931−935.
(38) Choi, H.; Chen, W. T.; Kamat, P. V. Know thy nano neighbor. Plasmonic versus electron charging effects of metal nanoparticles in dye-sensitized solar cells. *ACS Nano* **2012**, *6* (5), 4418−4427.
(39) Fahim, N.; Ouyang, Z.; Zhang, Y.; Jia, B.; Shi, Z.; Gu, M. Efficiency enhancement of screen-printed multicrystalline silicon solar cells by integrating gold nanoparticles via a dip coating process. *Opt. Mater. Express* **2012**, *2* (2), 190−204.
(40) Saha, S. K.; Guchhait, A.; Pal, A. J. $Cu_2ZnSnS_4$ (CZTS) nanoparticle based nontoxic and earth-abundant hybrid pn-junction solar cells. *Phys. Chem. Chem. Phys.* **2012**, *14* (22), 8090−8096.
(41) (a) Todorov, T. K.; Reuter, K. B.; Mitzi, D. B. High-efficiency solar cell with earth-abundant liquid-processed absorber. *Adv. Mater.* **2010**, *22* (20), E156−E159. (b) Ito, K.; Nakazawa, T. Electrical and optical properties of stannite-type quaternary semiconductor thin-films. *Jpn. J. Appl. Phys., Part 1* **1988**, *27* (11), 2094−2097. (c) Katagiri, H.; Jimbo, K.; Maw, W. S.; Oishi, K.; Yamazaki, M.; Araki, H.; Takeuchi, A. Development of CZTS-based thin film solar cells. *Thin Solid Films* **2009**, *517* (7), 2455−2460.
(42) Xin, X.; He, M.; Han, W.; Jung, J.; Lin, Z. Low-cost copper zinc tin sulfide counter electrodes for high-efficiency dye-sensitized solar cells. *Angew. Chem., Int. Ed.* **2011**, *50* (49), 11739−11742.
(43) Steinhagen, C.; Panthani, M. G.; Akhavan, V.; Goodfellow, B.; Koo, B.; Korgel, B. A. Synthesis of $Cu_2ZnSnS_4$ nanocrystals for use in low-cost photovoltaics. *J. Am. Chem. Soc.* **2009**, *131* (35), 12554−12555.
(44) Guo, Q.; Ford, G. M.; Yang, W.-C.; Walker, B. C.; Stach, E. A.; Hillhouse, H. W.; Agrawal, R. Fabrication of 7.2% efficient CZTSSe solar cells using CZTS nanocrystals. *J. Am. Chem. Soc.* **2010**, *132* (49), 17384−17386.
(45) Ford, G. M.; Guo, Q.; Agrawal, R.; Hillhouse, H. W. Earth abundant element $Cu_2Zn(Sn_{1-x}Ge_x)S_4$ nanocrystals for tunable bandgap solar cells: 6.8% Efficient device fabrication. *Chem. Mater.* **2011**, *23* (10), 2626−2629.
(46) Barkhouse, D. A. R.; Gunawan, O.; Gokmen, T.; Todorov, T. K.; Mitzi, D. B. Device characteristics of a 10.1% hydrazine-processed $Cu_2ZnSn(Se,S)_4$ solar cell. *Prog. Photovoltaics* **2012**, *20* (1), 6−11.
(47) Ni, M.; Leung, M. K. H.; Leung, D. Y. C.; Sumathy, K. A review and recent developments in photocatalytic water-splitting using for hydrogen production. *Renewable Sustainable Energy Rev.* **2007**, *11* (3), 401−425.
(48) Chen, X.; Li, C.; Grätzel, M.; Kostecki, R.; Mao, S. S. Nanomaterials for renewable energy production and storage. *Chem. Soc. Rev.* **2012**, *41* (23), 7909−7937.
(49) Li, Y.; Zhang, J. Z. Hydrogen generation from photoelectrochemical water splitting based on nanomaterials. *Laser Photonics Rev.* **2010**, *4* (4), 517−528.
(50) Hoyle, R.; Sotomayor, J.; Will, G.; Fitzmaurice, D. Visible-light-induced and long-lived charge separation in a transparent nanostructured semiconductor membrane modified by an adsorbed electron donor and electron acceptor. *J. Phys. Chem. B* **1997**, *101* (50), 10791−10800.
(51) (a) Khan, S. U. M.; Akikusa, J. Stability and photoresponse of nanocrystalline *n*-$TiO_2$ and *n*-$TiO_2/Mn_2O_3$ thin film electrodes during water splitting reactions. *J. Electrochem. Soc.* **1998**, *145* (1), 89−93. (b) Khan, S. U. M.; Akikusa, J. Photoelectrochemical splitting of water at nanocrystalline *n*-$Fe_2O_3$ thin-film electrodes. *J. Phys. Chem. B* **1999**, *103* (34), 7184−7189. (c) Ingler, W. B., Jr.; Baltrus, J. P.; Khan, S. U. M. Photoresponse of p-type zinc-doped iron(III) oxide thin films. *J. Am. Chem. Soc.* **2004**, *126* (33), 10238−10239.
(52) Miller, E. L.; Rocheleau, R. E.; Khan, S. A hybrid multijunction photoelectrode for hydrogen production fabricated with amorphous silicon/germanium and iron oxide thin films. *Int. J. Hydrogen Energy* **2004**, *29* (9), 907−914.
(53) Khan, S. U.; Al-Shahry, M.; Ingler, W. B. Efficient photochemical water splitting by a chemically modified n-$TiO_2$. *Science* **2002**, *297* (5590), 2243−2245.
(54) (a) Fujishima, A. Comment on "Efficient photochemical water splitting by a chemically modified *n*-$TiO_2$". *Science* **2003**, *301*, 1673a. (b) Hagglund, C.; Gratzel, M.; Kasemo, B. Comment on "Efficient photochemical water splitting by a chemically modified *n*-$TiO_2$". *Science* **2003**, *301*, 1673b. (c) Lackner, K. S. Comment on "Efficient photochemical water splitting by a chemically modified *n*-$TiO_2$". *Science* **2003**, 1673c 301.
(55) (a) Kongkanand, A.; Martínez Domínguez, R.; Kamat, P. V. Single wall carbon nanotube scaffolds for photoelectrochemical solar cells. Capture and transport of photogenerated electrons. *Nano Lett.* **2007**, *7* (3), 676−680. (b) Shankar, K.; Basham, J. I.; Allam, N. K.; Varghese, O. K.; Mor, G. K.; Feng, X.; Paulose, M.; Seabold, J. A.; Choi, K.-S.; Grimes, C. A. Recent advances in the use of $TiO_2$ nanotube and nanowire arrays for oxidative photoelectrochemistry. *J. Phys. Chem. C* **2009**, *113* (16), 6327−6359. (c) Varghese, O. K.; Grimes, C. A. Appropriate strategies for determining the photoconversion efficiency of water photoelectrolysis cells: A review with examples using titania nanotube array photoanodes. *Sol. Energy Mater. Sol. Cells* **2008**, *92* (4), 374−384. (d) Kitano, M.; Hara, M. Heterogeneous photocatalytic cleavage of water. *J. Mater. Chem.* **2010**, *20* (4), 627−641.
(56) Shaban, Y.; Khan, S. M. Carbon modified (CM)-*n*-$TiO_2$ thin films for efficient water splitting to $H_2$ and $O_2$ under xenon lamp light and natural sunlight illuminations. *J. Solid State Electrochem.* **2009**, *13* (7), 1025−1036.
(57) Maeda, K.; Teramura, K.; Lu, D.; Takata, T.; Saito, N.; Inoue, Y.; Domen, K. Photocatalyst releasing hydrogen from water. *Nature* **2006**, *440* (7082), 295−295.
(58) (a) Maeda, K.; Teramura, K.; Lu, D.; Saito, N.; Inoue, Y.; Domen, K. Noble-metal/$Cr_2O_3$ core/shell nanoparticles as a cocatalyst for photocatalytic overall water splitting. *Angew. Chem.* **2006**, *118* (46), 7970−7973. (b) Maeda, K.; Teramura, K.; Lu, D.; Saito, N.; Inoue, Y.; Domen, K. Roles of Rh/$Cr_2O_3$ (core/shell) nanoparticles photodeposited on visible-light-responsive $(Ga_{1-x}Zn_x)(N_{1-x}O_x)$ solid solutions in photocatalytic overall water splitting. *J. Phys. Chem. C* **2007**, *111* (20), 7554−7560. (c) Maeda, K.; Sakamoto, N.; Ikeda, T.; Ohtsuka, H.; Xiong, A.; Lu, D.; Kanehara, M.; Teranishi, T.; Domen, K. Preparation of core−shell-structured nanoparticles (with a noble-metal or metal oxide core and a chromia shell) and their application in water splitting by means of visible light. *Chem.−Eur. J.* **2010**, *16* (26), 7750−7759.
(59) (a) Vayssieres, L.; Beermann, N.; Lindquist, S.-E.; Hagfeldt, A. Controlled aqueous chemical growth of oriented three-dimensional

crystalline nanorod arrays: Application to iron(III) oxides. *Chem. Mater.* **2000**, *13* (2), 233−235. (b) Lindgren, T.; Wang, H.; Beermann, N.; Vayssieres, L.; Hagfeldt, A.; Lindquist, S.-E. Aqueous photoelectrochemistry of hematite nanorod array. *Sol. Energy Mater. Sol. Cells* **2002**, *71* (2), 231−243.

(60) (a) Khan, S. U. M.; Sultana, T. Photoresponse of *n*-$TiO_2$ thin film and nanowire electrodes. *Sol. Energy Mater. Sol. Cells* **2003**, *76* (2), 211−221. (b) Wolcott, A.; Smith, W. A.; Kuykendall, T. R.; Zhao, Y.; Zhang, J. Z. Photoelectrochemical water splitting using dense and aligned $TiO_2$ nanorod arrays. *Small* **2009**, *5* (1), 104−111.

(61) Ahn, K.-S.; Shet, S.; Deutsch, T.; Jiang, C.-S.; Yan, Y.; Al-Jassim, M.; Turner, J. Enhancement of photoelectrochemical response by aligned nanorods in ZnO thin films. *J. Power Sources* **2008**, *176* (1), 387−392.

(62) Ding, Q.-P.; Yuan, Y.-P.; Xiong, X.; Li, R.-P.; Huang, H.-B.; Li, Z.-S.; Yu, T.; Zou, Z.-G.; Yang, S.-G. Enhanced photocatalytic water splitting properties of $KNbO_3$ nanowires synthesized through hydrothermal method. *J. Phys. Chem. C* **2008**, *112* (48), 18846−18848.

(63) Wang, X.; Liu, G.; Chen, Z.-G.; Li, F.; Lu, G. Q.; Cheng, H.-M. Efficient and stable photocatalytic $H_2$ evolution from water splitting by $(Cd_{0.8}Zn_{0.2})S$ nanorods. *Electrochem. Commun.* **2009**, *11* (6), 1174−1178.

(64) Yan, S.; Wan, L.; Li, Z.; Zou, Z. Facile temperature-controlled synthesis of hexagonal $Zn_2GeO_4$ nanorods with different aspect ratios toward improved photocatalytic activity for overall water splitting and photoreduction of $CO_2$. *Chem. Commun.* **2011**, *47* (19), 5632−5634.

(65) Corma, A.; Atienzar, P.; Garcia, H.; Chane-Ching, J.-Y. Hierarchically mesostructured doped $CeO_2$ with potential for solar-cell use. *Nat. Mater.* **2004**, *3* (6), 394−397.

(66) (a) Wang, D.-Y.; Lin, H.-C.; Yen, C.-C. Influence of metal plasma ion implantation on photo-sensitivity of anatase $TiO_2$ thin films. *Thin Solid Films* **2006**, *515* (3), 1047−1052. (b) Yen, C.-C.; Wang, D.-Y.; Shih, M.-H.; Chang, L.-S.; Shih, H. C. A combined experimental and theoretical analysis of Fe-implanted $TiO_2$ modified by metal plasma ion implantation. *Appl. Surf. Sci.* **2010**, *256* (22), 6865−6870.

(67) Marschall, R.; Mukherji, A.; Tanksale, A.; Sun, C.; Smith, S. C.; Wang, L.; Lu, G. Q. Preparation of new sulfur-doped and sulfur/nitrogen co-doped $CsTaWO_6$ photocatalysts for hydrogen production from water under visible light. *J. Mater. Chem.* **2011**, *21* (24), 8871−8879.

(68) Asahi, R.; Morikawa, T.; Ohwaki, T.; Aoki, K.; Taga, Y. Visible-light photocatalysis in nitrogen-doped titanium oxides. *Science* **2001**, *293* (5528), 269−271.

(69) Irie, H.; Watanabe, Y.; Hashimoto, K. Nitrogen-concentration dependence on photocatalytic activity of $TiO_{2-x}N_x$ powders. *J. Phys. Chem. B* **2003**, *107* (23), 5483−5486.

(70) Ihara, T.; Miyoshi, M.; Iriyama, Y.; Matsumoto, O.; Sugihara, S. Visible-light-active titanium oxide photocatalyst realized by an oxygen-deficient structure and by nitrogen doping. *Appl. Catal., B* **2003**, *42* (4), 403−409.

(71) Serpone, N. Is the bandgap of pristine $TiO_2$ narrowed by anion- and cation-doping of titanium dioxide in second-generation photocatalysts? *J. Phys. Chem. B* **2006**, *110* (48), 24287−24293.

(72) Mitoraj, D.; Kisch, H. The nature of nitrogen-modified titanium dioxide photocatalysts active in visible light. *Angew. Chem., Int. Ed.* **2008**, *47* (51), 9975−9978.

(73) Chen, H. M.; Chen, C. K.; Liu, R. S.; Zhang, L.; Zhang, J.; Wilkinson, D. P. Nano-architecture and material designs for water splitting photoelectrodes. *Chem. Soc. Rev.* **2012**, *41* (17), 5654−5671.

(74) Youngblood, W. J.; Lee, S.-H. A.; Kobayashi, Y.; Hernandez-Pagan, E. A.; Hoertz, P. G.; Moore, T. A.; Moore, A. L.; Gust, D.; Mallouk, T. E. Photoassisted overall water splitting in a visible light-absorbing dye-sensitized photoelectrochemical cell. *J. Am. Chem. Soc.* **2009**, *131* (3), 926−927.

(75) (a) Chen, H. M.; Chen, C. K.; Chang, Y.-C.; Tsai, C.-W.; Liu, R.-S.; Hu, S.-F.; Chang, W.-S.; Chen, K.-H. Quantum dot monolayer sensitized ZnO nanowire-array photoelectrodes: True efficiency for water splitting. *Angew. Chem.* **2010**, *122* (34), 6102−6105. (b) Chen, H. M.; Chen, C. K.; Lin, C. C.; Liu, R.-S.; Yang, H.; Chang, W.-S.; Chen, K.-H.; Chan, T.-S.; Lee, J.-F.; Tsai, D. P. Multi-bandgap-sensitized ZnO nanorod photoelectrode arrays for water splitting: An X-ray absorption spectroscopy approach for the electronic evolution under solar illumination. *J. Phys. Chem. C* **2011**, *115* (44), 21971−21980.

(76) Thimsen, E.; Le Formal, F.; Grätzel, M.; Warren, S. C. Influence of plasmonic Au nanoparticles on the photoactivity of $Fe_2O_3$ electrodes for water splitting. *Nano Lett.* **2010**, *11* (1), 35−43.

(77) Gomes Silva, C.; Juárez, R.; Marino, T.; Molinari, R.; García, H. Influence of excitation wavelength (UV or visible light) on the photocatalytic activity of titania containing gold nanoparticles for the generation of hydrogen or oxygen from water. *J. Am. Chem. Soc.* **2010**, *133* (3), 595−602.

(78) Liu, Z.; Hou, W.; Pavaskar, P.; Aykol, M.; Cronin, S. B. Plasmon resonant enhancement of photocatalytic water splitting under visible illumination. *Nano Lett.* **2011**, *11* (3), 1111−1116.

(79) Ramsurn, H.; Gupta, R. B. Production of biocrude from biomass by acidic subcritical water followed by alkaline supercritical water two-step liquefaction. *Energy Fuels* **2012**, *26* (4), 2365−2375.

(80) *Renewable Fuel Standard (RFS)*; U.S. Environmental Protection Agency, 2011.

(81) Annual Energy Review 2011; Report No. DOE/EIA-0384(2011); U.S. Department of Energy, 2012.

(82) Gupta, R. B.; Demirbas, A. *Gasoline, Diesel and Ethanol Biofuels from Grasses and Plants*; Cambridge University Press: 2010.

(83) Vertes, A. A.; Qureshi, N.; Blaschek, H. P.; Yukawa, H. *Biomass to Biofuels: Strategies for Global Industries*; John Wiley & Sons, Ltd.: Chichester, United Kingdom, 2010.

(84) Cheng, S.; D'cruz, I.; Wang, M.; Leitch, M.; Xu, C. Highly efficient liquefaction of woody biomass in hot-compressed alcohol-water co-solvents. *Energy Fuels* **2010**, *24* (9), 4659−4667.

(85) Pattarkine, M.; Pattarkine, V. Nanotechnology for Algal Biofuels. In *The Science of Algal Fuels*; Gordon, R., Seckbach, J., Eds.; Springer: The Netherlands: 2012; Vol. 25, pp 147−163.

(86) (a) Li, C.; Yoshimoto, M.; Fukunaga, K.; Nakao, K. Characterization and immobilization of liposome-bound cellulase for hydrolysis of insoluble cellulose. *Bioresour. Technol.* **2007**, *98* (7), 1366−1372. (b) Moxley, G.; Zhu, Z.; Zhang, Y.-H. P. Efficient sugar release by the cellulose solvent-based lignocellulose fractionation technology and enzymatic cellulose hydrolysis. *J. Agric. Food Chem.* **2008**, *56* (17), 7885−7890.

(87) Cruz, J. C.; Pfromm, P. H.; Tomich, J. M.; Rezac, M. E. Conformational changes and catalytic competency of hydrolases adsorbing on fumed silica nanoparticles: I. Tertiary structure. *Colloids Surf., B* **2010**, *79* (1), 97−104.

(88) Wang, Y.; Hsieh, Y. L. Immobilization of lipase enzyme in polyvinyl alcohol (PVA) nanofibrous membranes. *J. Membr. Sci.* **2008**, *309* (1−2), 73−81.

(89) Lin, V.; Mahoney, P.; Gibson, K. Nanofarming Technology Extracts Biofuel Oil without harming Algae. http://www.ameslab.gov/news/news-releases/nanofarming-technology-extracts-biofuel-oil-without-harming-algae (accessed May 24, 2013)..

(90) Valenstein, J. S.; Kandel, K.; Melcher, F.; Slowing, I. I.; Lin, V. S. Y.; Trewyn, B. G. Functional mesoporous silica nanoparticles for the selective sequestration of free fatty acids from microalgal oil. *ACS Appl. Mater. Interfaces* **2012**, *4* (2), 1003−1009.

(91) Venkat Reddy, C. R.; Oshel, R.; Verkade, J. G. Room-temperature conversion of soybean oil and poultry fat to biodiesel catalyzed by nanocrystalline calcium oxides. *Energy Fuels* **2006**, *20* (3), 1310−1314.

(92) Montero, J.; Wilson, K.; Lee, A. Cs Promoted triglyceride transesterification over MgO nanocatalysts. *Top. Catal.* **2010**, *53* (11−12), 737−745.

(93) Deng, X.; Fang, Z.; Liu, Y.-h.; Yu, C.-L. Production of biodiesel from Jatropha oil catalyzed by nanosized solid basic catalyst. *Energy* **2011**, *36* (2), 777−784.

(94) Tang, S.; Wang, L.; Zhang, Y.; Li, S.; Tian, S.; Wang, B. Study on preparation of $Ca/Al/Fe_3O_4$ magnetic composite solid catalyst and

its application in biodiesel transesterification. *Fuel Process. Technol.* **2012**, *95*, 84−89.
(95) Saunders, J. R.; Benfield, D.; Moussa, W.; Amirfazli, A. Nanotechnology's implications for select systems of renewable energy. *Int. J. Green Energy* **2007**, *4*, 483−503.
(96) Abuadala, A.; Dincer, I.; Naterer, G. F. Exergy analysis of hydrogen production from biomass gasification. *Int. J. Hydrogen Energy* **2010**, *35* (10), 4981−4990.
(97) Hao, X.; Guo, L.; Zhang, X.; Guan, Y. Hydrogen production from catalytic gasification of cellulose in supercritical water. *Chem. Eng. J.* **2005**, *110* (1−3), 57−65.
(98) Taylor, A. D.; DiLeo, G. J.; Sun, K. Hydrogen production and performance of nickel based catalysts synthesized using supercritical fluids for the gasification of biomass. *Appl. Catal., B* **2009**, *93* (1−2), 126−133.
(99) Lestari, S.; Mäki-Arvela, P.; Beltramini, J.; Lu, G.; Murzin, D. Y. Transforming triglycerides and fatty acids into biofuels. *ChemSusChem* **2009**, *2* (12), 1109−1119.
(100) Richardson, Y.; Blin, J.; Volle, G.; Motuzas, J.; Julbe, A. In situ generation of Ni metal nanoparticles as catalyst for $H_2$-rich syngas production from biomass gasification. *Appl. Catal., A* **2010**, *382* (2), 220−230.
(101) Devi, L.; Ptasinski, K. J.; Janssen, F. J. J. G. A review of the primary measures for tar elimination in biomass gasification processes. *Biomass Bioenergy* **2003**, *24* (2), 125−140.
(102) Han, J.; Kim, H. The reduction and control technology of tar during biomass gasification/pyrolysis: An overview. *Renewable Sustainable Energy Rev.* **2008**, *12* (2), 397−416.
(103) Li, J.; Yan, R.; Xiao, B.; Liang, D. T.; Du, L. Development of nano-NiO/$Al_2O_3$ catalyst to be used for tar removal in biomass gasification. *Environ. Sci. Technol.* **2008**, *42* (16), 6224−6229.
(104) Li, J.; Yan, R.; Xiao, B.; Liang, D. T.; Lee, D. H. Preparation of nano-NiO particles and evaluation of their catalytic activity in pyrolyzing biomass components. *Energy Fuels* **2007**, *22* (1), 16−23.
(105) (a) De, S.; Dutta, S.; Patra, A. K.; Bhaumik, A.; Saha, B. Self-assembly of mesoporous $TiO_2$ nanospheres via aspartic acid templating pathway and its catalytic application for 5-hydroxymethyl-furfural synthesis. *J. Mater. Chem.* **2011**, *21* (43), 17505−17510. (b) Dutta, S.; De, S.; Patra, A. K.; Sasidharan, M.; Bhaumik, A.; Saha, B. Microwave assisted rapid conversion of carbohydrates into 5-hydroxymethylfurfural catalyzed by mesoporous $TiO_2$ nanoparticles. *Appl. Catal., A* **2011**, *409*, 133−139.
(106) Dutta, S.; De, S.; Saha, B. A Brief summary of the synthesis of polyester building-block chemicals and biofuels from 5-hydroxymethylfurfural. *ChemPlusChem* **2012**, *77* (4), 259−272.
(107) Manzer, L. E. Biomass Derivatives: A Sustainable Source of Chemicals. In *Feedstocks for the Future: Renewables for the Production of Chemicals and Materials*; Bozell, J. J.; Patel, M. K., Eds.; ACS Symposium Series 921; American Chemical Society: Washington, DC, 2006; Chapter 4, pp 40−51.
(108) Taarning, E.; Nielsen, I. S.; Egeblad, K.; Madsen, R.; Christensen, C. H. Chemicals from renewables: Aerobic oxidation of furfural and hydroxymethylfurfural over gold catalysts. *ChemSusChem* **2008**, *1* (1−2), 75−78.
(109) Casanova, O.; Iborra, S.; Corma, A. Biomass into chemicals: Aerobic oxidation of 5-hydroxymethyl-2-furfural into 2,5-furandicarboxylic acid with gold nanoparticle catalysts. *Chemsuschem* **2009**, *2* (12), 1138−1144.
(110) Davis, S. E.; Houk, L. R.; Tamargo, E. C.; Datye, A. K.; Davis, R. J. Oxidation of 5-hydroxymethylfurfural over supported Pt, Pd and Au catalysts. *Catal. Today* **2011**, *160* (1), 55−60.
(111) Gupta, N. K.; Nishimura, S.; Takagaki, A.; Ebitani, K. Hydrotalcite-supported gold-nanoparticle-catalyzed highly efficient base-free aqueous oxidation of 5-hydroxymethylfurfural into 2,5-furandicarboxylic acid under atmospheric oxygen pressure. *Green Chem.* **2011**, *13* (4), 824−827.
(112) Pasini, T.; Piccinini, M.; Blosi, M.; Bonelli, R.; Albonetti, S.; Dimitratos, N.; Lopez-Sanchez, J. A.; Sankar, M.; He, Q.; Kiely, C. J. Selective oxidation of 5-hydroxymethyl-2-furfural using supported gold−copper nanoparticles. *Green Chem.* **2011**, *13* (8), 2091−2099.
(113) Garcia-Suarez, E. J.; Balu, A. M.; Tristany, M.; Garcia, A. B.; Philippot, K.; Luque, R. Versatile dual hydrogenation−oxidation nanocatalysts for the aqueous transformation of biomass-derived platform molecules. *Green Chem.* **2012**, *14*, 1434−1439.
(114) Pushkarev, V. V.; Musselwhite, N.; An, K.; Alayoglu, S.; Somorjai, G. A. High structure sensitivity of vapor-phase furfural decarbonylation/hydrogenation reaction network as a function of size and shape of Pt nanoparticles. *Nano Lett.* **2012**, *12* (10), 5196−5201.
(115) Clark, J. H.; Yoshida, K.; Gai, P. L. Efficient aqueous hydrogenation of biomass platform molecules using supported metal nanoparticles on Starbons®. *Chem. Commun.* **2009**, *35*, 5305−5307.
(116) Yan, N.; Zhao, C.; Luo, C.; Dyson, P. J.; Liu, H.; Kou, Y. One-step conversion of cellobiose to $C_6$-alcohols using a ruthenium nanocluster catalyst. *J. Am. Chem. Soc.* **2006**, *128* (27), 8714−8715.
(117) Crossley, S.; Faria, J.; Shen, M.; Resasco, D. E. Solid nanoparticles that catalyze biofuel upgrade reactions at the water/oil interface. *Science* **2010**, *327* (5961), 68−72.
(118) Xu, X.; Li, Y.; Gong, Y.; Zhang, P.; Li, H.; Wang, Y. Synthesis of palladium nanoparticles supported on mesoporous N-doped carbon and their catalytic ability for biofuel upgrade. *J. Am. Chem. Soc.* **2012**, *134* (41), 16987−16990.
(119) Zapata, P. A.; Faria, J.; Ruiz, M. P.; Resasco, D. E. Condensation/hydrogenation of biomass-derived oxygenates in water/oil emulsions stabilized by nanohybrid catalysts. *Top. Catal.* **2012**, *55* (1−2), 38−52.
(120) Chang, A. C. C.; Louh, R. F.; Wong, D.; Tseng, J.; Lee, Y. S. Hydrogen production by aqueous-phase biomass reforming over carbon textile supported Pt−Ru bimetallic catalysts. *Int. J. Hydrogen Energy* **2011**, *36* (14), 8794−8799.
(121) Roy, D.; Subramaniam, B.; Chaudhari, R. V. Aqueous phase hydrogenolysis of glycerol to 1,2-propanediol without external hydrogen addition. *Catal. Today* **2010**, *156* (1−2), 31−37.
(122) Kim, H.-D.; Park, H. J.; Kim, T.-W.; Jeong, K.-E.; Chae, H.-J.; Jeong, S.-Y.; Lee, C.-H.; Kim, C.-U. The effect of support and reaction conditions on aqueous phase reforming of polyol over supported Pt−Re bimetallic catalysts. *Catal. Today* **2012**, *185* (1), 73−80.
(123) Guo, Y.; Azmat, M. U.; Liu, X.; Wang, Y.; Lu, G. Effect of support's basic properties on hydrogen production in aqueous-phase reforming of glycerol and correlation between WGS and APR. *Appl. Energy* **2012**, *92*, 218−223.
(124) Dietrich, P.; Lobo-Lapidus, R.; Wu, T.; Sumer, A.; Akatay, M. C.; Fingland, B.; Guo, N.; Dumesic, J.; Marshall, C.; Stach, E.; Jellinek, J.; Delgass, W. N.; Ribeiro, F.; Miller, J. Aqueous phase glycerol reforming by PtMo bimetallic nano-particle catalyst: Product selectivity and structural characterization. *Top. Catal.* **2012**, *55* (1−2), 53−69.
(125) Kim, H.-D.; Park, H. J.; Kim, T.-W.; Jeong, K.-E.; Chae, H.-J.; Jeong, S.-Y.; Lee, C.-H.; Kim, C.-U. Hydrogen production through the aqueous phase reforming of ethylene glycol over supported Pt-based bimetallic catalysts. *Int. J. Hydrogen Energy* **2012**, *37* (10), 8310−8317.
(126) Jin, X.; Dang, L.; Lohrman, J.; Subramaniam, B.; Ren, S.; Chaudhari, R. V. Lattice-matched bimetallic CuPd-graphene nanocatalysts for facile conversion of biomass-derived polyols to chemicals. *ACS Nano* **2013**, *7* (2), 1309−1316.
(127) Sun, J.; Mei, D.; Karim, A. M.; Datye, A. K.; Wang, Y. Minimizing the formation of coke and methane on Co nanoparticles in steam reforming of biomass-derived oxygenates. *ChemCatChem* **2013**, DOI: 10.1002/cctc.201300041.
(128) Maeda, K.; Domen, K. Photocatalytic water splitting: Recent progress and future challenges. *J. Phys. Chem. Lett.* **2010**, *1* (18), 2655−2661.
(129) Helgesen, M.; Søndergaard, R.; Krebs, F. C. Advanced materials and processes for polymer solar cell devices. *J. Mater. Chem.* **2009**, *20* (1), 36−60.